Journal of Arid Environments 232 (2026) 105500

Contents lists available at ScienceDirect

Journal of Arid Environments

journal homepage: www.elsevier.com/locate/jaridenv

Spatio-temporal dynamics of vegetation and water bodies in the Lake Urmia Basin (1984–2022): an analysis using MODIS and Landsat data with new perspective

Javid Hojabri [a,*], Thong Nguyen-Huy [b,c,**]

[a] Department of Remote Sensing and GIS, University of Tehran, Tehran, Iran
[b] Centre for Applied Climate Sciences, University of Southern Queensland, Toowoomba, QLD, 4350, Australia
[c] Faculty of Information Technology, Thanh Do University, Kim Chung, Hoai Duc, Ha Noi, 100000, Viet Nam

ARTICLE INFO

Keywords:
Lake Urmia
Basin
Dams
Vegetation
NDVI
NDWI
Threshold

ABSTRACT

This study aims to quantitatively analyze the spatio-temporal changes in Lake Urmia's surface area, vegetation cover, and dam reservoirs from 1984 to 2022, using Landsat and MODIS data to comprehensively understand long-term environmental changes in the Lake Urmia Basin (ULB), northwest Iran. Landsat images from 15 selected years between 1984 and 2022, and MODIS data from August for each year 2000–2022, were used. The Normalized Difference Water Index (NDWI) and Normalized Difference Vegetation Index (NDVI) were used to assess long time water bodies and vegetation dynamics. Unlike previous studies that rely solely on conventional NDVI thresholding, this research not only uses conventional NDVI thresholding but also introduces several novel sampling-based approaches to improve classification accuracy. Conventional NDVI-based vegetation thresholds, along with newly developed methods based on representative sample pixels, were used to identify high-vigor vegetation, low-vigor vegetation, and non-vegetated areas. For lakes and reservoirs, the NDWI and sample pixels were used to separate water from non-water areas. The analysis revealed a substantial decline in Lake Urmia's surface area, decreasing from 491,597 ha in 1984 to 189,719 ha in 2022, with the most severe reduction observed in 2014 and 2015 (≈ 88 % decrease). In contrast, the area of water reservoirs behind dams increased from 4,788 ha to 8,118 ha over the same period. Vegetation cover expanded significantly, with MODIS-derived analysis indicating increases of 2.11 times in 2020 and 1.8 times in 2022 compared to 2000. Area of high-vigor vegetation which means vegetation with high index (NDVI 0.65–1) showed 13.51 times increase in 2020 and 6.81 times in 2022. Statistical analysis revealed a negative relationship between vegetation area and lake area, with correlation coefficients ranging from −0.71 to −0.32. These findings highlight the simultaneous expansion of vegetation and dam reservoirs alongside the continued shrinkage of Lake Urmia, suggesting significant hydrological and land cover changes in the basin over recent decades. Notably, this study covers a 38-year period from 1984 to 2022, making it one of the longest continuous analyses of the LUB. Therefore, policymakers and relevant authorities must make informed, data-driven decisions to prevent further deterioration of the region's hydrological and ecological conditions.

1. Introduction

Iran, largely classified as an arid and semi-arid country, features a narrow wet and rainy region in the north contrasting with vast arid deserts in its central parts (Dehshiri, 2018; Shifteh Some'e et al., 2013). The Lake Urmia basin (LUB) is one of the six primary catchment basins in Iran with Lake Urmia at its center (Taheri Dehkordi et al., 2022). This unique and valuable lake faces a looming threat of desiccation, reminiscent of the Aral Sea catastrophe (AghaKouchak et al., 2015). While both human and non-human factors contribute to its decline, evidence and research point towards human activities as the primary drivers. Key contributors include dam construction, highway development, excessive agriculture, and irresponsible irrigation (Alizade Govarchin Ghale et al., 2018; Barhagh et al., 2021; Mojtahedi et al., 2022; Schulz et al., 2020;

* Corresponding author.
** Corresponding author. Centre for Applied Climate Sciences, University of Southern Queensland, Toowoomba, QLD, 4350, Australia.
E-mail addresses: Javidhojabri@gmail.com (J. Hojabri), Thong.Nguyen-Huy@unisq.edu.au (T. Nguyen-Huy).

https://doi.org/10.1016/j.jaridenv.2025.105500
Received 30 May 2025; Received in revised form 3 October 2025; Accepted 4 October 2025
Available online 16 October 2025

Shams Ghahfarokhi and Moradian, 2023). The decline in lake level accelerated significantly after 1995, primarily due to the construction of dams on 13 major rivers feeding the lake (Hassanzadeh et al., 2012; Jalili et al., 2016). These dams have greatly impacted the basin's agriculture and hydrology, causing changes in cultivation patterns and increased water consumption for agricultural, urban, and industrial purposes (Majediasl and Sangi, 2013; Shadkam et al., 2016; Sima et al., 2021).

The shrinkage of Lake Urmia has profoundly impacted its local environment and communities, while also illustrating globally the ecological and socio-economic consequences of saline-lake desiccation. Like the catastrophic decline of the Aral Sea, Urmia's retreat has coincided with salt storms, health issues linked to high salinity, and soil salinization (Delavar et al., 2020; Feizizadeh et al., 2023; Ghale et al., 2021). These parallel underscores the broader relevance of such ecological crises and the urgent need for monitoring and mitigation efforts. As with communities neighboring the Aral Sea, the drying of Lake Urmia has brought severe economic strain, reduced food production, degraded soil quality, heightened disease prevalence, mass migration, and related challenges (Anchita et al., 2021; Barani Pesyan et al., 2017; Feizizadeh et al., 2022; Jafari-Khounigh et al., 2022). Moreover, these impacts extend beyond the basin, affecting approximately 76 million people across a 500 km radius that includes parts of Iran, Azerbaijan, Armenia, Iraq, and Turkey, emphasizing the regional and global stakes involved (Garousi et al., 2013; Pengra, 2012).

The shrinkage of Lake Urmia has multiple causes. Some studies attribute it to dam construction (Barış, 2023; Memarian Sorkhabi and Kurdpour, 2024), others to agricultural expansion in the basin (AghaKouchak et al., 2015; Barideh and Nasimi, 2022; Ghale et al., 2019; Naboureh et al., 2021), and some to climate change (Kanani et al., 2020; Shadkam et al., 2016). Additionally, some research points to the construction of the Kalantari causeway as another factor (Hemmati et al., 2021; Wurtsbaugh and Sima, 2022). Nevertheless, some aspects of lake's decline remained unclear. Thus, this basin requires more comprehensive research to assess the main factors contributing to the lake's shrinkage. Given the LUB's extensive area of 52,000 km^2, satellite imagery is essential for assessing spatiotemporal changes in the basin. Over the past years, extensive research has been conducted on the various issues about Lake Urmia, and its basin with a strong emphasis on satellite images and remote sensing techniques. These studies focused on hydrological changes and evapotranspiration (Tasumi, 2019), land use and surface temperature dynamics (Emami and Zarei, 2021; Feizizadeh et al., 2013; Hojabri and Aydin, 2025), soil salinity (Delavar et al., 2020; Mirzaee et al., 2024), human activities impacts on the lake and basin (Hosseini-Moghari et al., 2020; Mojtahedi et al., 2022), and dust and aerosol pollution (Boroughani et al., 2019; Delfi et al., 2019). Satellite data are widely used to study Lake Urmia and its basin because they offer long-term historical coverage, cost-effective data acquisition, and broad spatial reach with minimal effort. This enables monitoring of temporal changes in water surface area, agriculture, temperature, salinity, dust activity, and other basin-scale environmental variables.

The crisis in the LUB is largely attributed to the expansion of vegetation and agricultural lands over the years, as well as the increasing water demand for irrigation in agricultural lands (Ghale et al., 2019; Hesami and Amini, 2016; Shirmohammadi et al., 2020). Some studies have utilized satellite imagery, especially Landsat and MODIS data, to explore the condition of water and vegetation changes over time. For instance, Hesami and Amini (2016) utilized Landsat (TM) data and official records to assess the irrigation area expansion and water consumption in the southeast region of the LUB. The findings indicated a 20 % rise in irrigated area, and a 35 % increase in water demand for irrigation during 1989–2000. Shadkam et al. (2016) showed a 37 % increase in irrigated lands from 1970 to 2010. According to Koushki (2013), between 1979 and 2011 the lake's area declined from 494,700 ha to 232,300 ha, while the irrigated area increased from 158,523 ha to 450,000 ha. Another study by Naboureh et al. (2021) revealed between 1987 and 2020 the lake area decreased by 202,000 ha while the irrigated lands increased by 89,000 ha. Parsinejad et al. (2022) estimated water consumption for major crops in the basin by using Landsat and MODIS images, their study revealed that actual water consumption often exceeded irrigation needs. Yazdandoost and Moradian (2021) simulated future conditions from 2015 to 2050, using NDWI to illustrate lake area decline. Shams Ghahfarokhi and Moradian (2023) investigated lake changes from 1970 to 2020, using NDVI and NDWI to conclude that human factors had a greater impact on the current state of the lake compared to climate change and drought. Rahimi and Breuste (2021) analyzed the lake's condition from 1987 to 2014 and simulated its state in 2025 using Landsat time series data. Their findings revealed a 2 % decrease in area from 1987 to 2000, followed by a 28 % decrease from 2000 to 2010, and a rapid decline between 2010 and 2014.

Taheri Dehkordi et al. (2022), analyzed Landsat time series images using Google Earth Engine (GEE) to show a significant 60 % decrease in the water level between 1996 and 2016. Schröder et al. (2022) established a relationship between height, area, and volume of the lake using NDWI and MNDWI derived from Landsat data, with a threshold of 0.14 for water pixels. Tourian et al. (2015) by utilizing ENVISAT, CryoSat-2 altimetry, and MODIS data between 2002 and 2014 showed a 220 $\pm$ 6 km^2/year decrease in lake area. Also, a recent assessment using MODIS and Landsat data by Saemian et al. (2020) showed lake stabilization and a recovery phase from 2015 to 2019, with an annual increase of 14.5 cm in water level, 204 km^2 in area, and 0.42 km^3 in volume. Naboureh et al. (2021) combined NDWI and NDVI from Landsat and MODIS (1987–2020) to study agricultural impacts, they resulted in a 2020 km^2 decline in surface water, although some improvement was noted after 2015. However, over the years 1987–2019, the water level decreased by almost 5 m. Tarighi et al. (2023) applied ML to Landsat images (2012–2017) to classify shallow and deep water and observed a decreasing trend from 2012 to 2014, followed by recovery until 2018.

Most of the previous studies on the LUB have investigated vegetation dynamics, lake surface area variations, and dam construction impacts individually. Nonetheless, discrepancies among these findings (attributable to differing methodologies and data sources) highlight the necessity for an integrated, comprehensive assessment. The basin is transitioning from a semi-arid environment to an arid landscape characterized by the emergence of a large salt desert following the drying of Lake Urmia. Understanding the primary drivers behind this environmental shift is crucial for sustainable basin management and to prevent further deterioration.

This research aims to address this knowledge gap by conducting a holistic analysis of spatiotemporal changes in vegetation, water bodies, and anthropogenic modifications within the basin, utilizing MODIS and Landsat datasets spanning 1984 to 2022. Recognizing the limitations of traditional NDVI threshold-based classification methods such as fixed thresholds of 0.1 or 0.2 (Elgammal et al., 2014; Gandhi et al., 2015; Hashim et al., 2019), this study introduces innovative sampling-based approaches that target representative pixels of varying vegetation vigor and water bodies. These methods reduce inaccuracies caused by inter-annual NDVI variability, thereby enhancing the reliability of long-term environmental monitoring.

By employing pixel-based sampling, this study provides a more precise assessment of changes in Lake Urmia's surface area, vegetation cover, and reservoirs' extent over nearly four decades. Focusing on dry summer conditions further deepen ecological insights, elucidating the complex interactions under climatic and human-induced pressures.

Aligned with the journal's scope, this study offers key contributions to dryland environmental research:

1. Integrated analysis of vegetation dynamics, lake surface area, and reservoirs' extent in the basin.
2. Long-term trend analysis over a broad time frame to illuminate desertification and resilience.

3. Comparison of NDVI thresholding versus sampling-based classification methods, with improved accuracy.
4. Insights into the relationships among lake shrinkage, reservoirs expansion, and vegetation changes to guide sustainable management.

Ultimately, this research seeks to answer critical questions, including:

i. How have vegetation cover, lake surface area, and reservoirs' extent evolved from 1984 to 2022 in the LUB?
ii. How do sampling-based classification methods improve vegetation analysis accuracy?
iii. How are water body shrinkage, dam development, and vegetation dynamics interconnected, and what are their implications for sustainable basin management?

The overarching goal is to quantify environmental changes and refine monitoring methodologies, thereby contributing to ecological restoration and water resource management strategies in arid and semi-arid regions globally.

2. Materials and methodology

2.1. Study area

Located in northwest Iran, the LUB covers approximately 52,700 km^2 across East Azerbaijan, West Azerbaijan, and Kurdistan provinces (see Fig. 1). It is characterized by a semi-arid climate, mountainous terrain, and significant agricultural activity (Barideh and Nasimi, 2022; Eimanifar and Mohebbi, 2007; Hosseini-Moghari et al., 2020). The region experiences seasonal precipitation primarily from October to May, marked by hot summers, cold winters, and high evaporation rates that significantly impact water availability (Darehshouri et al., 2023; Djamali et al., 2008). Supporting approximately 6.4 million residents, the basin's economy relies heavily on agriculture, which constitutes a vital sector. It covers 8.47 % of Iran's farmland and is dominated by irrigated crops, rangelands, and horticulture, including key products such as grapes, apples, and wheat (Feizizadeh et al., 2022). Lake Urmia, a large hypersaline, terminal lake within the basin, historically spanned over 5, 700 km^2 but has experienced significant shrinkage due to reduced inflows, dam constructions, and climate factors (Jalili et al., 2016). It is fed by 13 main rivers, with water loss primarily through evaporation, making it a critical ecological and climatic regulator in the region (Ghaheri et al., 1999).

2.2. Satellite imagery

This study utilized Landsat 5, Landsat 8, and Landsat 9 satellite imagery obtained from the USGS Earth Explorer data archive. Images selected were of high quality, with cloud cover less than 10 %, covering the period from 1984 to 2022. The specific acquisition years included 1984, 1990, 2000, 2006, 2007, 2009–2011, 2013–2017, 2020, and 2022. Landsat data was chosen for its long-term availability and consistent 30-m spatial resolution, which is suitable for monitoring environmental changes over extended periods.

To ensure comparability, all images were acquired during August, a month characterized by minimal cloud cover and representative of the vegetation conditions in the basin. August was selected because the vegetation and green cover during this period primarily depend on irrigation, given the region's summer drought conditions and negligible natural precipitation, which prevents significant natural vegetation growth without irrigation. To minimize temporal discrepancies between images, all images within each imaging column were selected to be from

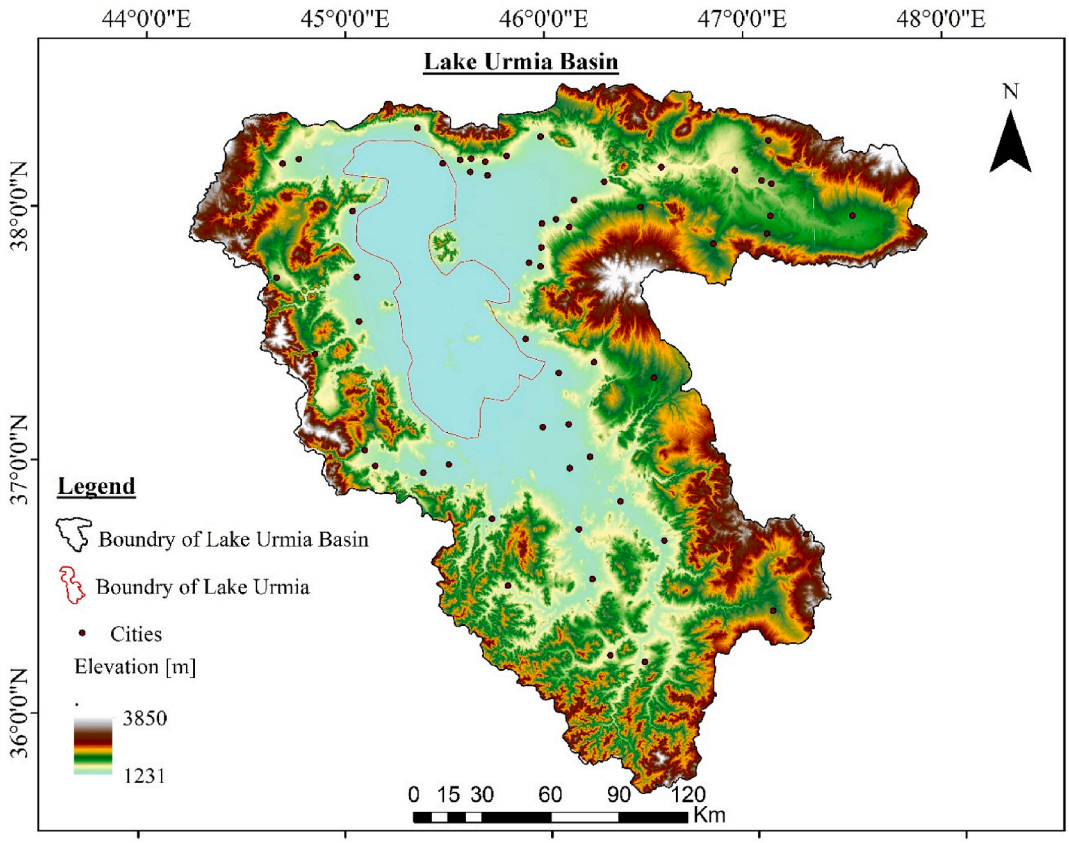

Fig. 1. Geographical position of the LUB, boundary of Lake Urmia and elevations (m).

the same acquisition date (see Table A.1 in the Appendix). A total of seven Landsat scenes (see Fig. 2), covering paths 167–169 and rows 33–35, were required to fully encompass the LUB.

Additionally, this study utilizes the MODIS/Terra Vegetation product (MOD13Q1), version 6, in which images are taken every 16 days at a spatial resolution of 250 m. A total of 23 MOD13Q1 products were downloaded for the period from August 2000 to 2022, focusing on data collected between August 13 and 29 (the mean interval of 16 days). The data were obtained from the LAADS DAAC (DAAC, 2023).

2.3. Ground-based data

Basin-wide temperature and precipitation data were obtained to analyze climate trends. These data served as a contextual layer for understanding the observed changes in vegetation and water bodies. Furthermore, historical lake water level data were used for altimetry analysis to quantify the decreasing trend in the lake's water volume.

2.4. Reference data for validation

Google Earth images were used to assist in accurate sampling and validation of vegetation and water pixels identified in the false color composite layers and NDVI layers. The spatial resolution of the Google Earth imagery used varies depending on the available data, typically ranging from approximately 15 m for high-resolution satellite images to 30 m for some older or lower-resolution images. All polygons created for sampling and clipping, which contained sample pixels in ArcMap, were converted to KML format and imported into Google Earth for accuracy verification. Google Earth data were only used in years for which historical data of Google Earth for August of that year were available for the LUB.

Table 1 summarized the data used in this research.

2.5. Remote sensing indices

The Normalized Difference Vegetation Index (NDVI) (Equation (1)) and the Normalized Difference Water Index (NDWI) (Equation (2)) are essential remote sensing tools used to monitor environmental conditions. NDVI, calculated from the difference between near-infrared (NIR) and red reflectance, ranges from −1 to +1 and is used to assess vegetation health and coverage, with higher values indicating healthier, denser green vegetation. Conversely, NDWI, derived from green and NIR reflectance, also ranges from −1 to +1 but is used to identify water bodies, with positive values indicating water surfaces and non-positive values representing non-water areas. In the context of the study, NDVI was employed to evaluate vegetation dynamics within the basin, while NDWI was utilized to analyze changes in water coverage over the years from 1984 to 2022, providing valuable insights into the spatial and

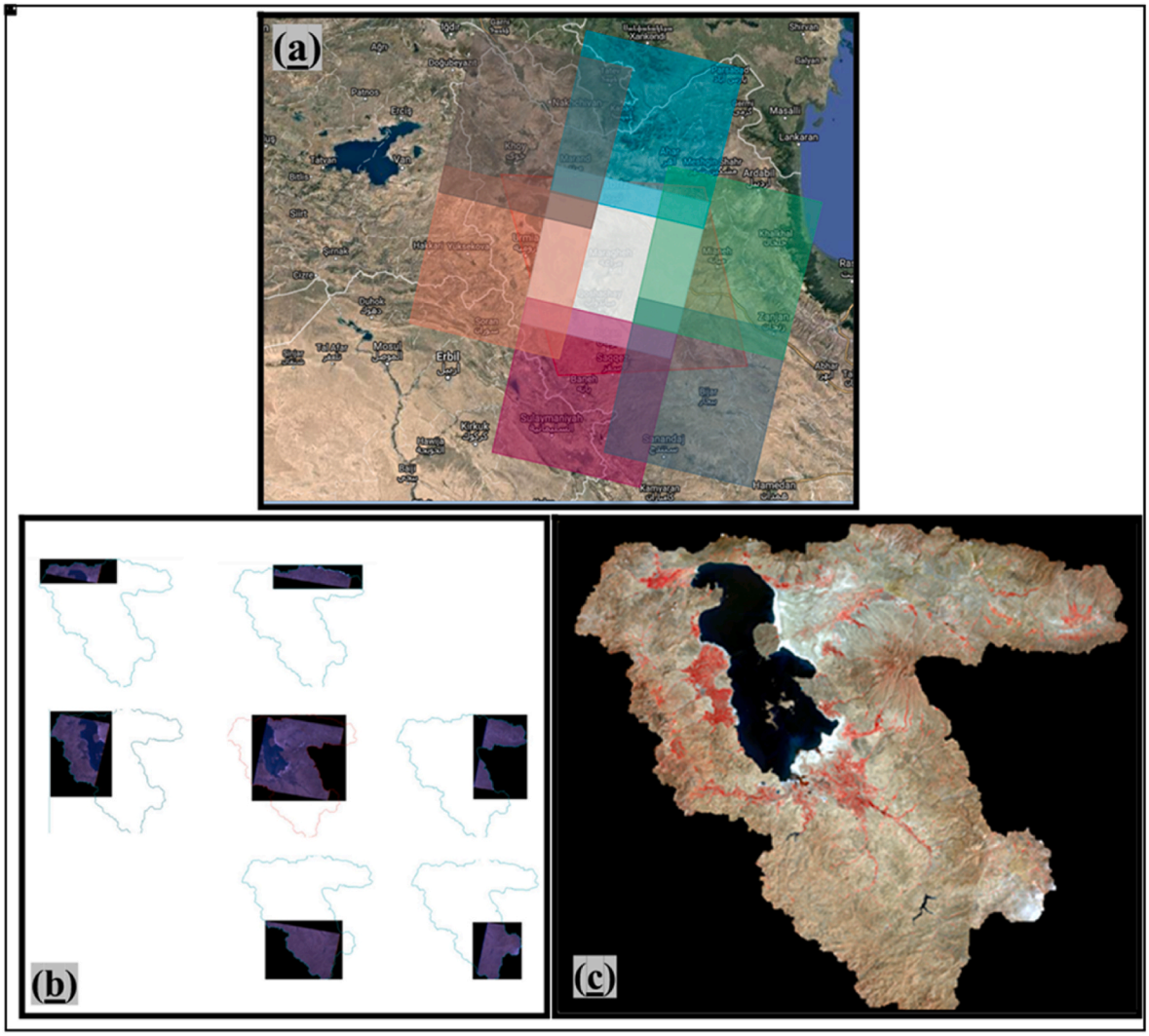

Fig. 2. (a) Display of seven Landsat images that cover the whole area of LUB (US Geological website). (b) Cropped area from each of the Landsat images based on the boundary of the basin in ENVI software. (c) Mosaiced image of LUB in ERDAS IMAGINE software (year 1984).

Table 1
The dataset used in our study.

Data	Resolution (m)	Study Period	Studied months	Data Format	Source	URL
Landsat 5	30	1984 to 2011	August	GeoTIFF	USGS	earthexplorer.usgs.gov
Landsat 8	30	2011 to 2022	August	GeoTIFF	USGS	earthexplorer.usgs.gov
Landsat 9	30	2022	August	GeoTIFF	USGS	earthexplorer.usgs.gov
Google Earth	15–30 m	1984 to 2022	August	KML	USGS	earth.google.com
MODIS (MOD13Q1)	250 m	2000 to 2022	August	HDF	LAADS DAAC	Find Data - LAADS DAAC
Lake water level	–	1984 to 2022	August	Text	Iran Meteorological Organization (IMO)	www.irimo.ir
Precipitation	–	1984 to 2022	Whole months	Text	Previous Studies	–
Temperature	–	1984 to 2022	August	Text	Previous Studies	–

temporal variations of both vegetation and water resources.

$$NDVI = (NIR - Red)/(NIR + RED) \quad (1)$$

$$NDWI = (Green - NIR)/(Green + NIR) \quad (2)$$

2.6. Analysis of water bodies in the basin

The water bodes was analyzed with Landsat images only. At first, preprocessing was performed on all Landsat images (a total of 105 images, i.e., 7 scenes × 15 years) (See supplementary file for details). Image preprocessing and mosaicking were carried out using ENVI and ERDAS IMAGINE software's, as illustrated in Fig. 2. The final product was a comprehensive, multi-temporal mosaic spanning 1984 to 2022, enabling consistent long-term analysis.

After calculating NDWI on 15 mosaiced image of basin, within the lake boundary, NDWI >0 classified water, while NDWI ≤0 classified as non-water, enabling lake area estimation. Then water pixels were validated against Google Earth imagery and false-color composites to set annual NDWI thresholds. Pixels above the threshold were classified as water, and those below but above zero as wet soil. To estimate reservoir storage, we subtracted the lake area from the total basin water extent (Equation (3)).

$$\text{Area of waters behind dams} = \text{all waters area in the LUB} - \text{water area in the lake area} \quad (3)$$

River water areas were ignored in the equation due to Landsat's spatial resolution limiting the detection of narrow rivers, their frequent dryness in August (exacerbated by dams), and their overall negligible area even in the study's initial years.

2.7. Vegetation analysis using MODIS data

NDVI layers from MOD13Q1 (August 2000–2022) were classified into three vegetation categories: low-vigor, moderate, and high-vigor (see glossary for definition). The process involved three steps: first, dividing NDVI into two classes (low-vigor: 0.2–0.3; moderate/high: 0.3–1); second, refining into three categories with adjusted thresholds (low-vigor: 0.35–0.5, moderate: 0.5–0.65, high-vigor: 0.65–1); and third, analyzing overall vegetation cover using MODIS data, focusing on NDVI values between 0.35 and 1 for total vegetation and 0.5–1 for high-vigor vegetation. Due to MODIS's 250-m resolution, detailed pixel-level analysis was unsuitable, so only these broader classifications were applied.

2.8. Vegetation analysis using landsat data

2.8.1. Conventional classification approach

For this analysis, data from 1984 to 2017 were obtained from level 1 images, while the images of 2020 and 2022 were derived from level 2 images. Therefore, the analysis focused on the period from 1984 to 2017 in this stage. After calculating the NDVI from Landsat images of the basin, the vegetation was categorized into three primary classes based on NDVI ranges: low-vigor vegetation (0.35–0.5), moderate vegetation (0.5–0.65), and high-vigor vegetation (0.65–1.0). Additionally, we implemented a more detailed classification scheme for moderate vegetation, subdividing this category into six minor classes with 0.05 intervals (0.35–0.40, 0.40–0.45, 0.45–0.50, 0.50–0.55, 0.55–0.60, and 0.60–0.65), while maintaining a broader classification for high-vigor vegetation (0.65–1). This approach enabled a comprehensive analysis of vegetation dynamics in the region.

2.8.2. Vegetation thresholding based on sample pixels

By overlaying the false-color composite layer of the basin using Landsat bands (to distinguish vegetation) with the NDVI layer in ArcMap for each study year, and cross-checking with historical Google Earth images, we selected a sufficient and representative number of sample pixels and classified them as non-vegetation, low-vigor vegetation, or high-vigor vegetation. At this stage, the maximum precision was adopted to select the most suitable areas as sample pixels and the polygons layer created from each of the categories of high-vigor vegetation, non-vegetation and low-vigor vegetation, in which every category had the least amount of impurity of other pixels (Figs. 3 and 4).

For each year separately sample pixels from three distinct classes of different regions of LUB, were selected carefully. Therefore, for each of the studied years, three groups of sample pixels of non-vegetation pixels, low-vigor vegetation pixels and high-vigor vegetation pixels were prepared with a certain and almost constant number in all the studied years. In the next step, the pixel value of all sample pixels in each category was extracted and sorted in ascending order.

Here are steps for selecting sample pixels:

1. Creating false color composite maps of the basin (by combining Nir, Red, and green bands) for each study year of basin.
2. Generating NDVI layers of basin for each study year.
3. Creating polygons precisely outlining areas of high-vigor vegetation, low-vigor-vegetation, and non-vegetation areas in ArcMap.
4. Converting these polygons to KML format for input into Google Earth (for checking samples accuracy).
5. If samples are acceptable within all polygons, proceeding with them; otherwise relocating the polygons with errors to suitable areas.
6. Clipping the NDVI layer using polygons for each sample category in ArcMap.
7. Extracted NDVI values for all three sample categories.

2.8.2.1. Threshold value derived from last non-vegetation pixel values. The approach of this method is to determine the vegetation threshold based on the pixel value of the last non-vegetation sample pixel. However, since each sample may contain some impurity pixels, we exclude the last 10 pixels of each non-vegetation samples. Then, we identify the largest remaining non-vegetation pixel among the remaining pixels and use its value as the vegetation threshold (red point in Fig. 5). To see the coding for this method, see the Appendix, Code A.1. (See supplementary file for details).

2.8.2.2. Threshold value using transition points. In this method, we classify NDVI using transition points. As illustrated in Fig. 5, there are

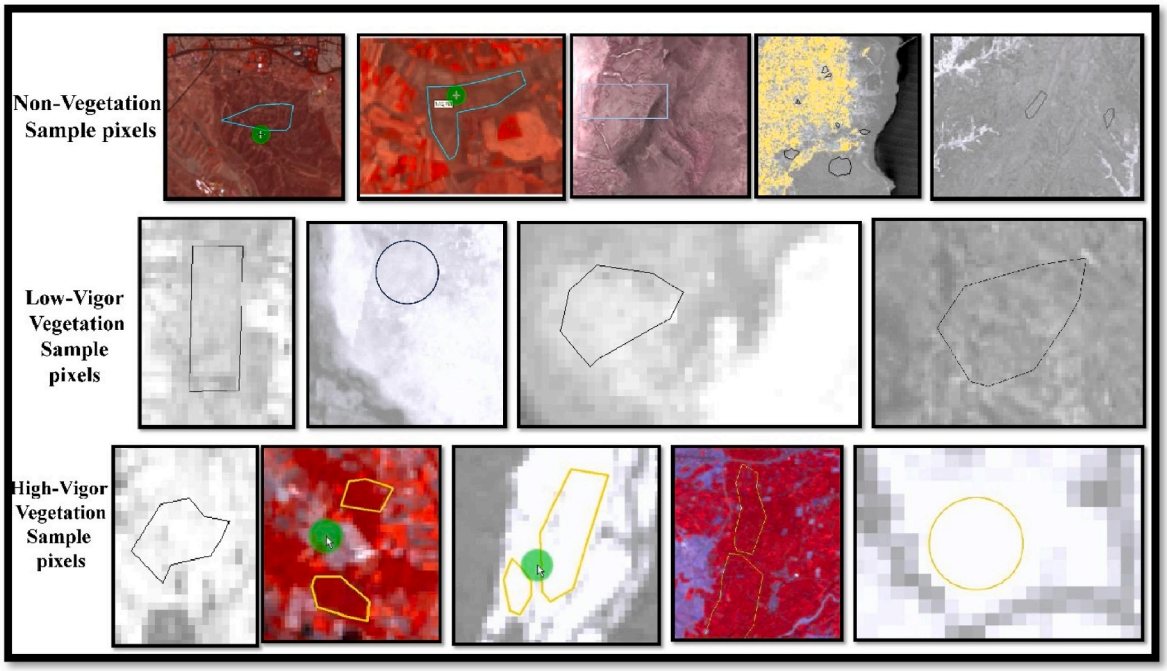

Fig. 3. Sample pixel selection of non-vegetation, low-vigor vegetation, and high-vigor vegetation pixels for each of the studied years using the false-color composite and NDVI layers of the basin. (For interpretation of the references to color in this figure legend, the reader is referred to the Web version of this article.)

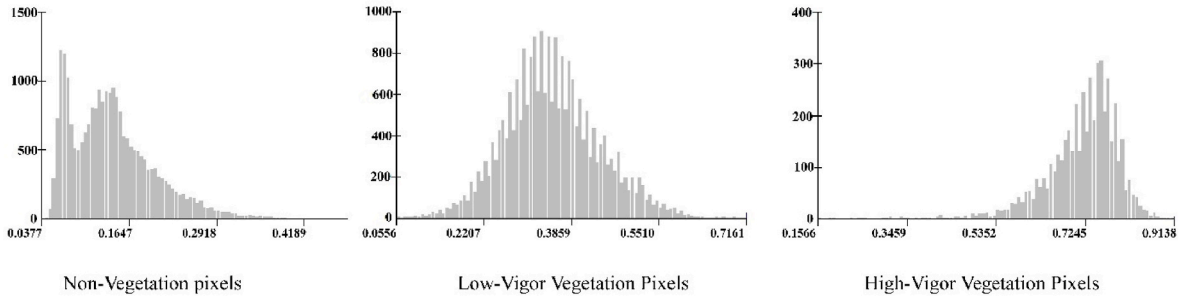

Fig. 4. Scatter plot showing the numerical values for non-vegetation, low-vigor vegetation, and high-vigor vegetation sample pixels for year 2010.

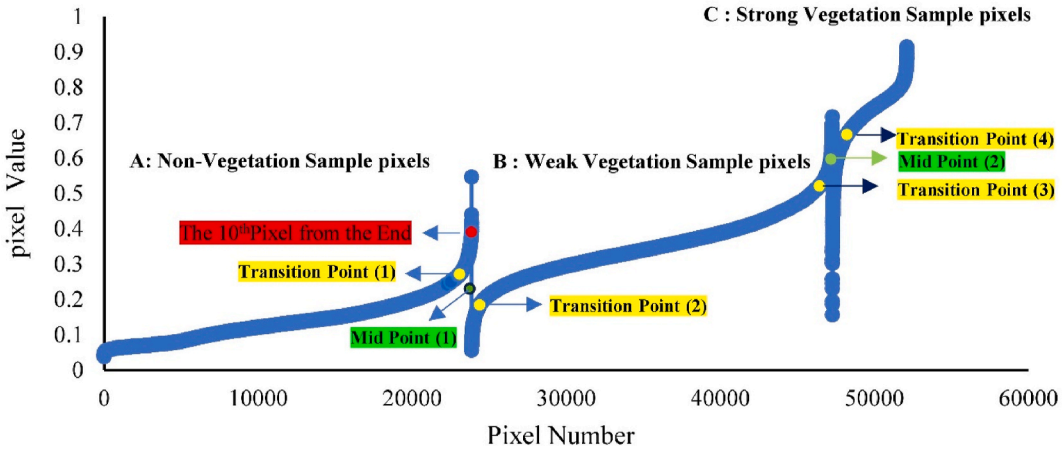

Fig. 5. Pixel values for non-vegetation, low-vigor, and high-vigor vegetation sample pixels in 2010. Curve A shows the vegetation threshold establishment: excluding the 10 pixels with the highest values and selecting the highest remaining pixel value as the threshold. Curves B and C illustrate key features, including transition points (1, 2, 3, and 4) and midpoints (1 and 2).

four transition points where the pixel types change to different pixel groups. Furthermore, the slope of the curves begins to change immediately following these points.

After these transition points, the pixel values shift to a higher class. Specifically, the differences in the Y-values of side-by-side pixels increase sharply at Transition Points (1) and (3), or decrease sharply at Transition Points (2) and (4). In this study, we considered Mid-point (2) and transition point (4) as threshold value. To see the coding for these methods are described in the Appendix, Code A.2. and A.3. (See supplementary file for details).

2.8.2.3. Fence-based threshold method. In this method, we used two threshold values: i) the average of non-vegetation pixels upper fence and high-vigor vegetation pixels lower fence (Fig. 6. (a) and Equation (4)), and ii) the average of low-vigor vegetation pixels upper fence and high-vigor vegetation pixels lower fence (Fig. 06. (b) and Equation (5)). These methods aim to remove outliers and impure pixel samples using the quartile. The coding for these methods is presented in the Appendix, Code A.4.

$$\begin{cases} \text{Upper fence}_{\text{non-vegetation}} = Q3_{nv} + (Q3_{nv} - Q1_{nv})*1.5 \\ \text{Lower fence}_{\text{High-vigor-vegetation}} = Q1_{Hvv} - (Q3_{Hvv} - Q1_{Hvv})*1.5 \end{cases} \quad (4)$$

$$\begin{cases} \text{Upper fence}_{\text{Low-vigor-vegetation}} = Q3_{Lvv} + (Q3_{Lvv} - Q1_{Lvv})*1.5 \\ \text{Lower fence}_{\text{High-vigor-vegetation}} = Q1_{Hvv} - (Q3_{Hvv} - Q1_{Hvv})*1.5 \end{cases} \quad (5)$$

Fig. 7 illustrates the overall workflow of the research, outlining the key steps undertaken from data collection and preprocessing to analysis and validation. Table 2 highlights the main differences between the conventional approach and the sample-based method, emphasizing variations in data requirements, accuracy, efficiency, and applicability to vegetation classification.

3. Results

3.1. Water body dynamics

Using the NDWI >0 threshold, the area of Lake Urmia decreased from 491,597 ha in 1984 to 189,719 ha in 2022. The maximum lake area was observed in 1990 at 503,394 ha, while the minimum occurred in 2015 at 128,343 ha, representing a 74.5 % decline from the peak (Fig. 8

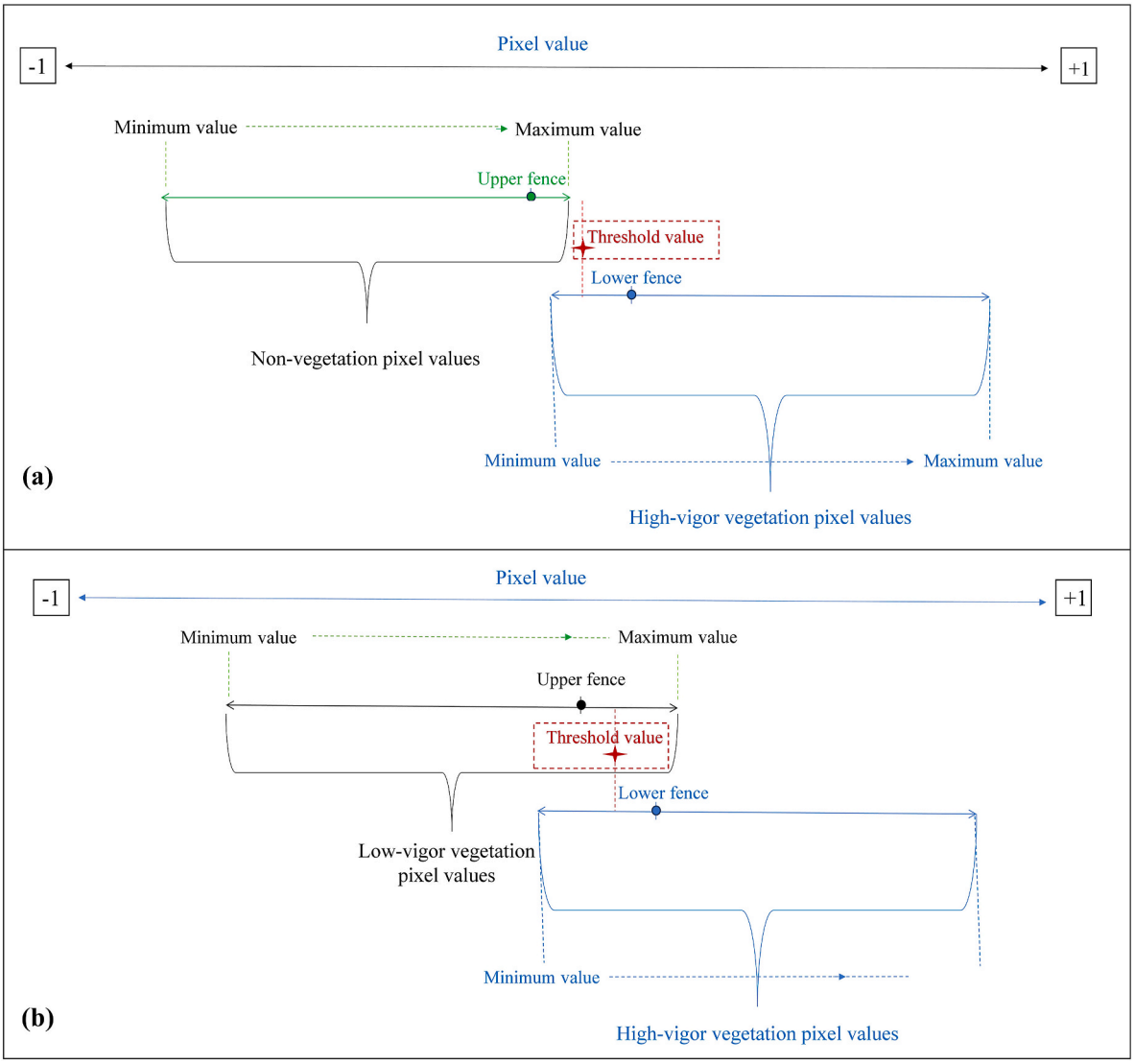

Fig. 6. (a) Finding the threshold value for vegetation by using an upper fence of non-vegetation sample pixels and a lower fence of high-vigor vegetation sample pixels. (b) Finding the threshold value for vegetation by using an upper fence of low-vigor-vegetation sample pixels and a lower fence of high-vigor vegetation sample pixels.

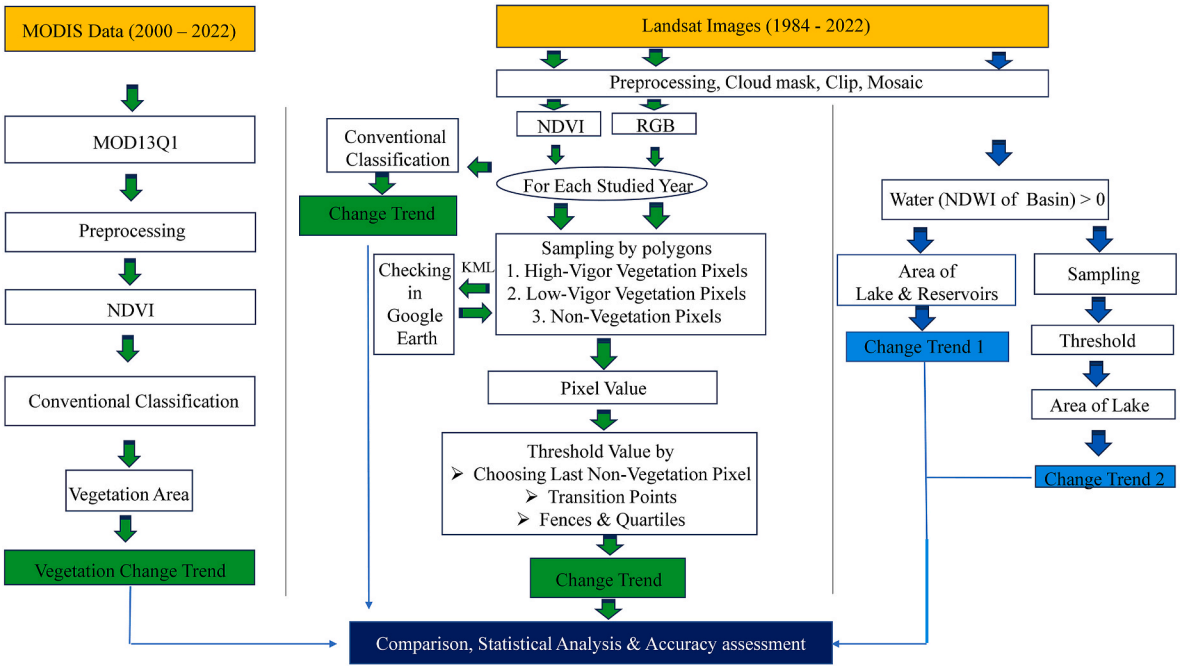

Fig. 7. Flowchart depicted the process carried out in this study.

Table 2
Comparison of two methods used in this study.

Feature/Action	Conventional NDVI thresholding	Sampling-based adaptive classification
Threshold determination	Apply fixed NDVI thresholds uniformly across all images	Individually determine optimal thresholds per image using sample pixels
Classification process	Classify vegetation using preset NDVI cutoff values	Define and adapt thresholds dynamically based on selected sample pixels value
Map generation	Generate maps using consistent, pre-set thresholds	Generate maps using year-specific, adaptive thresholds
Handling of variability	Limited; insensitive to year-to-year, seasonal, or atmospheric changes	Accounts for natural variability by customizing thresholds per image
Accuracy & robustness	Prone to misclassification under complex or varied conditions	Achieves higher accuracy and robustness through tailored thresholds
Overall approach	Conventional, static, threshold-dependent method	Innovative, dynamic, adaptive, sampling-based method
Feature/action	Conventional NDVI thresholding	Sampling-based adaptive classification

(a) and (e)).

Applying a sample-pixel threshold for refined lake water area further reduced the lake area to 55,673 ha in 2015, indicating an 88.83 % decrease from 1990 and a 75.22 % reduction from 1984 to 2022 (Fig. 8 (b) and (f)). Visual comparison of reservoir areas between 1984 and 2022 (Fig. 8(c) and (d)) shows a substantial increase in both the number and extent of reservoirs (Fig. 8(g)). Eventually, Fig. 8(h) shows lake elevation fluctuation in the years 1984–2022.

3.2. Vegetation dynamics

3.2.1. MODIS-based analysis

Fig. 9 presents vegetation classification maps derived from MODIS data using the conventional approach for the years 2000, 2020, and 2022, in two different classification way. First as shown in Fig. 9(a), which vegetation classified in two groups, vegetation cover within the LUB increased substantially between 2000 and 2022. Specifically, the Miandoab, Naqadeh, and Oshnavieh plains (indicated in zoomed area B) showed a notable expansion of the red vegetation class (NDVI 0.3–1.0). In another classification map, the spatial coverage of the green (NDVI 0.35–0.5), red (NDVI 0.5–0.65), and dark red (NDVI 0.65–1) vegetation classes also expanded during this period (Fig. 9(b)).

Between 2000 and 2022, the area of low-vigor vegetation (NDVI 0.2–0.3) in the LUB doubled, as shown in Fig. A.2. The total vegetation (NDVI 0.3–1) increased from 307,096 ha in 2000 to 555,461 ha in 2022, representing an 80 % growth (Fig. 10(a)). Moderate vegetation (NDVI 0.5–0.65) grew from 51,840 ha in 2000 to 154,028 ha in 2022, also a 197 % increase, with a maximum of 175,000.5 ha in 2020 (Fig. 10(b) and (d)). High-vigor vegetation (NDVI 0.65–1) showed the lowest spatial coverage in 2000, increasing steadily thereafter to reach its peak in 2020. Over this period, the area classified as high-vigor vegetation expanded significantly, increasing 13.5-fold by 2020 and 6.8-fold by 2022 compared to the 2000 level (Fig. 10(c) and (d)). Fig. 10(e) further shows that both high-vigor vegetation (NDVI 0.5–1) and total vegetation (NDVI 0.35–1) exhibited a steady upward trend, especially after the initial years of the study period.

3.2.2. Landsat-based analysis

Having confirmed the expansion of vegetation area around Lake Urmia using MODIS data, we further examined the corresponding changes with Landsat data, applying both conventional (Figs. 11 and 12) and sample-based methods (Figs. 13–16 and Tables 3–5). Fig. 11(a) shows that high-vigor vegetation (NDVI 0.65–1) increased significantly from 74,096.73 ha in 1984 to 148,956.7 ha in 2017, representing an approximately 101 % increase. Low-vigor vegetation (NDVI 0.35–0.5) displayed the lowest growth among the vegetation classes.

As illustrated in Fig. 11(b), total vegetation area (NDVI 0.35–1) was lowest in 2000 at 250,819 ha, before nearly doubling to a peak of 498,933 ha in 2016. The seven-class NDVI classification shown in Fig. 11(c) further highlights that high-vigor vegetation (NDVI 0.65–1) consistently exceeds other classes, except in 2000. Its area increased steadily from 74,096 ha in 1984 to 148,956 ha in 2017. Within the moderate NDVI range (0.35–0.65), the 0.35–0.4 class maintained the largest extent, while the 0.6–0.65 class remained the smallest across the study period. Fig. 12 displays the spatial distribution of three vegetation classes across the basin in 1984 and 2016.

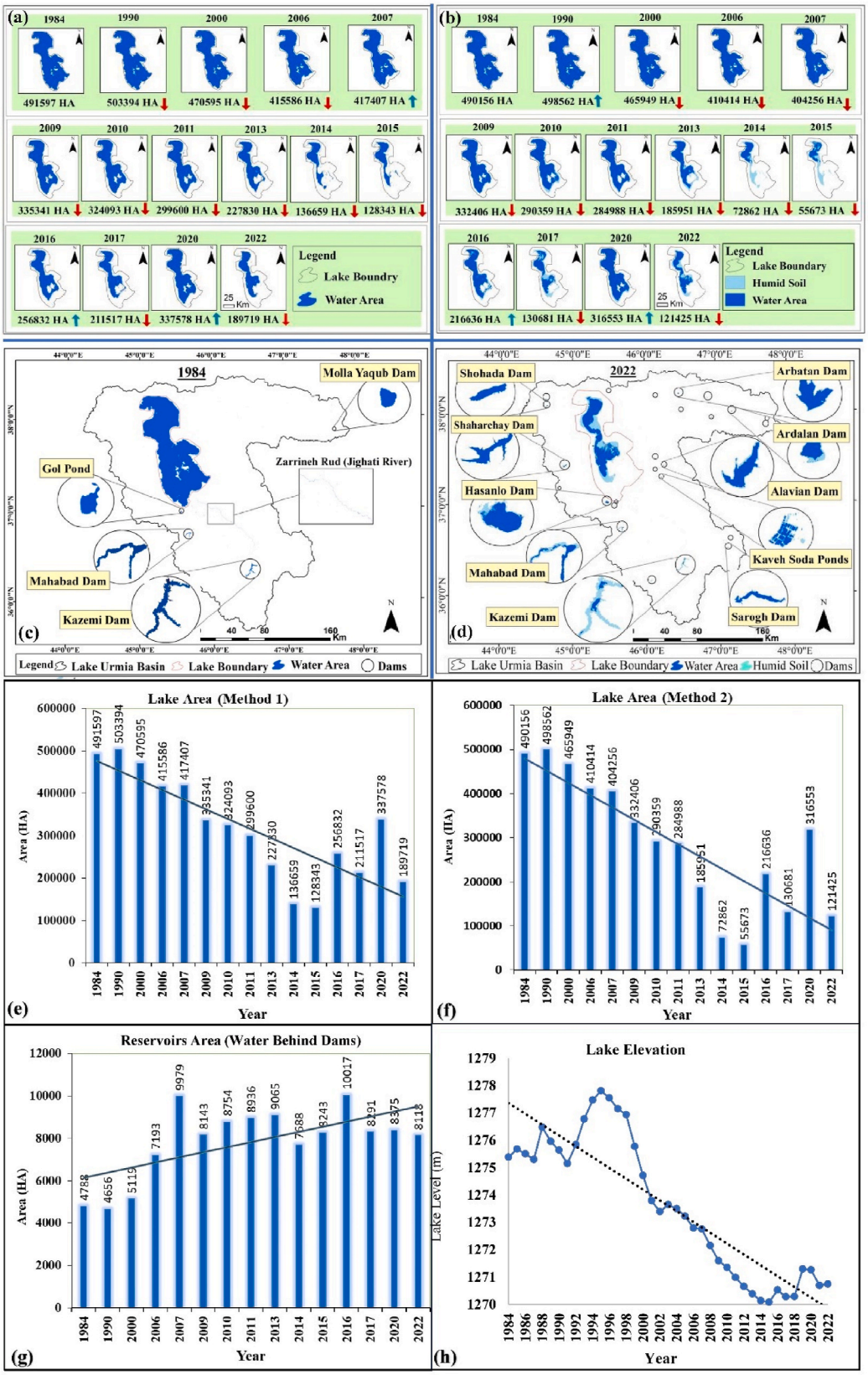

Fig. 8. (a) Time series map showing changes in the water extent of Lake Urmia from 1984 to 2022, derived from Landsat images using NDWI (NDWI >0). (b) Time series map generated from Landsat images and NDWI, employing sample pixels and a threshold for water detection. (c) Dam reservoirs in the LUB for the year 1984, identified from Landsat images and the NDWI index. (d) Dam reservoirs in the LUB for the year 2022, identified from Landsat images and the NDWI index. (e) Time series chart showing changes in the water extent of Lake Urmia from 1984 to 2022, derived from Landsat images using NDWI (NDWI >0). (f) Time series chart showing changes in the water extent of Lake Urmia from 1984 to 2022 by employing sample pixels as a threshold for water area. (g) The water extent of the existing dam reservoirs in the basin over time, obtained from the NDWI and Equation (3). (h) Lake water elevation from 1984 to 2022.

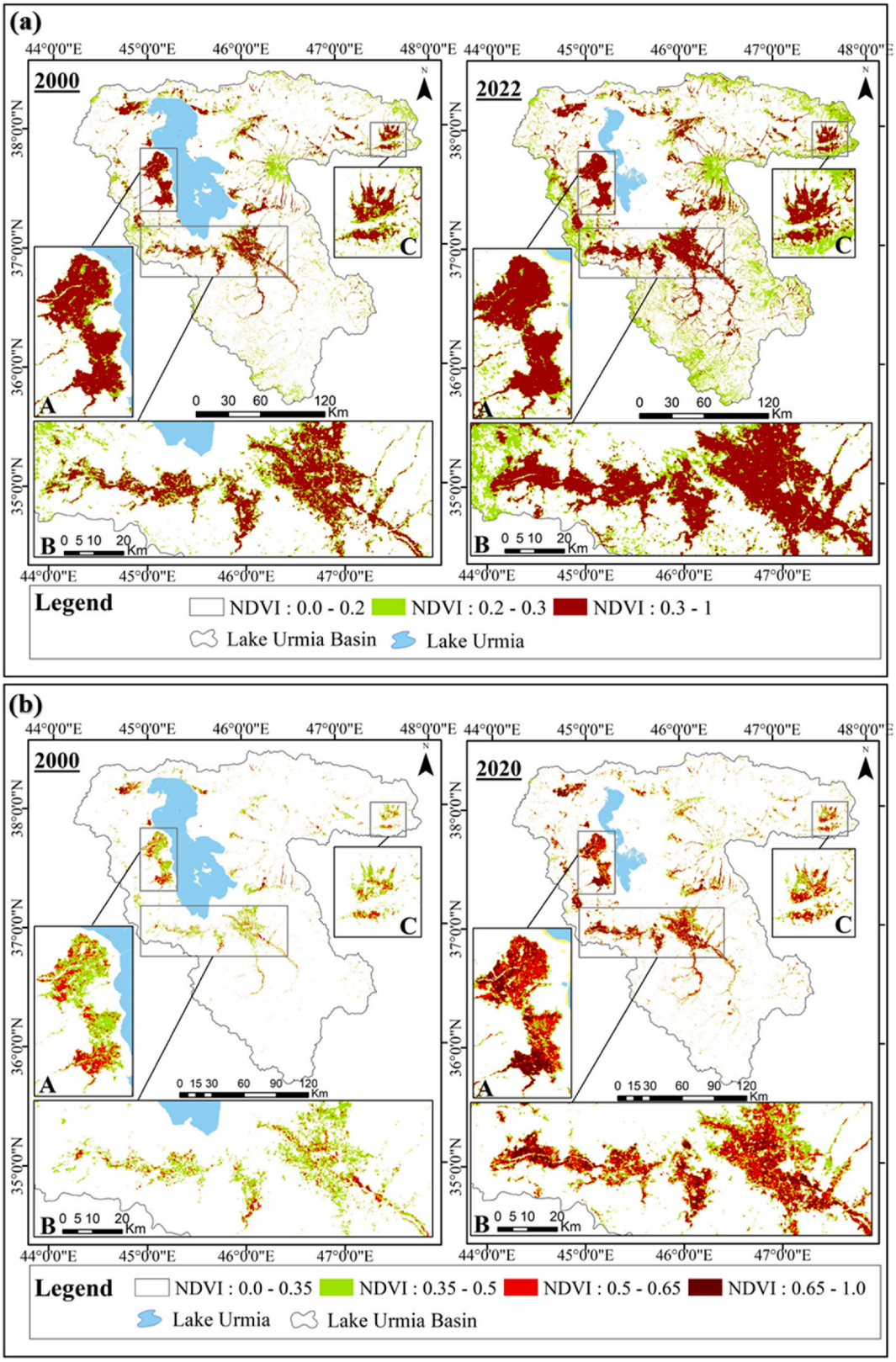

Fig. 9. Comparison of vegetation density and area in the basin using MODIS data and conventional classification between (a) 2000 and 2022, distinguishing low-vigor vegetation (NDVI 0.2–0.3) and total vegetation (NDVI 0.3–1); and (b) 2000 and 2020, distinguishing low-vigor vegetation (NDVI 0.35–0.5), moderate vegetation (NDVI 0.5–0.65), and high-vigor vegetation (NDVI 0.65–1).

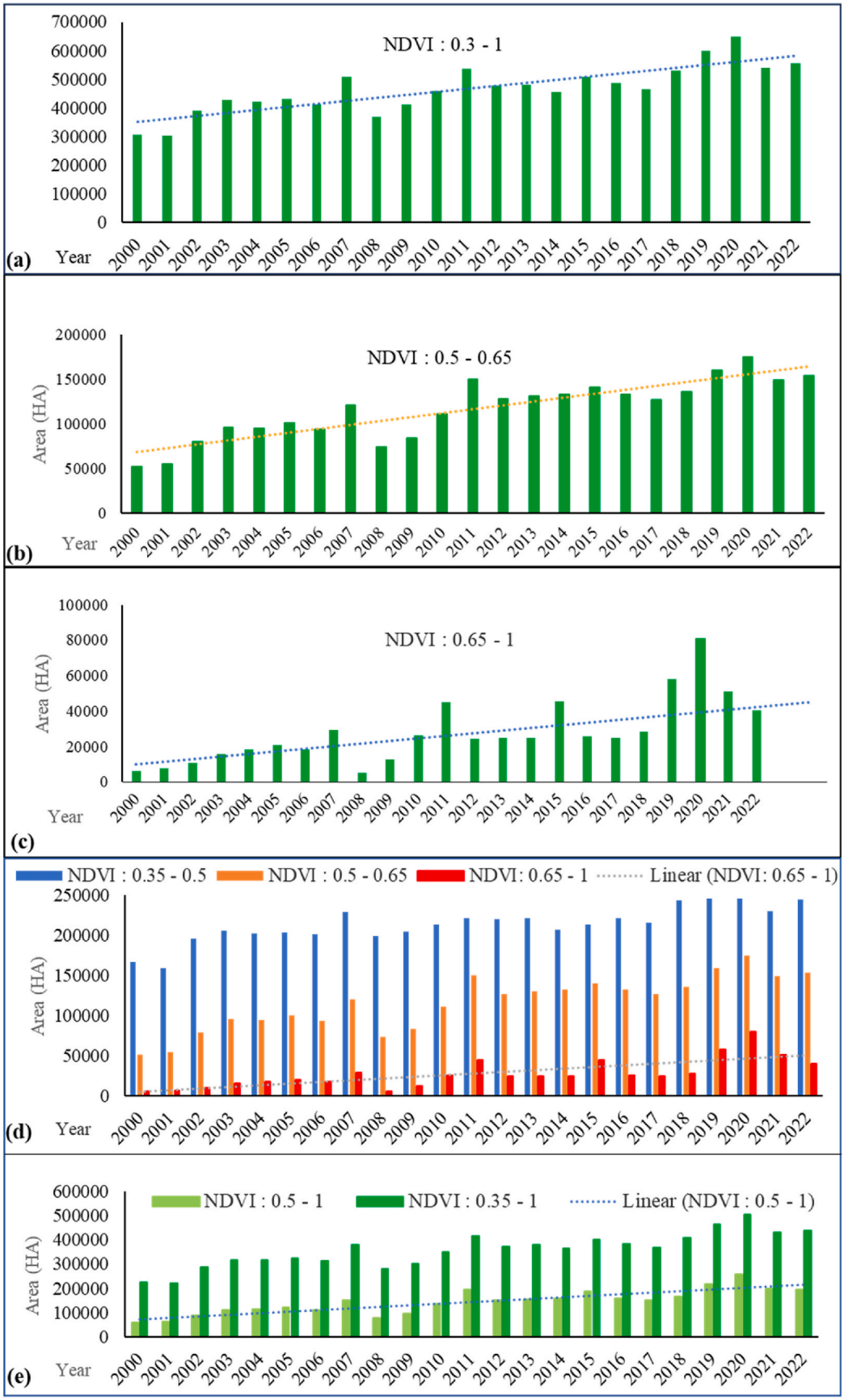

Fig. 10. Vegetation area changes in the basin from 2000 to 2022 based on MODIS products: (a) total vegetation (NDVI 0.3–1); (b) moderate vegetation (NDVI 0.5–0.65); (c) high-vigor vegetation (NDVI 0.65–1); (d) low-vigor vegetation (NDVI 0.35–0.5), moderate vegetation (NDVI 0.5–0.65) and high-vigor vegetation (NDVI 0.65–1); and (e) total vegetation (NDVI 0.35–1) and high-vigor vegetation (NDVI 0.5–1).

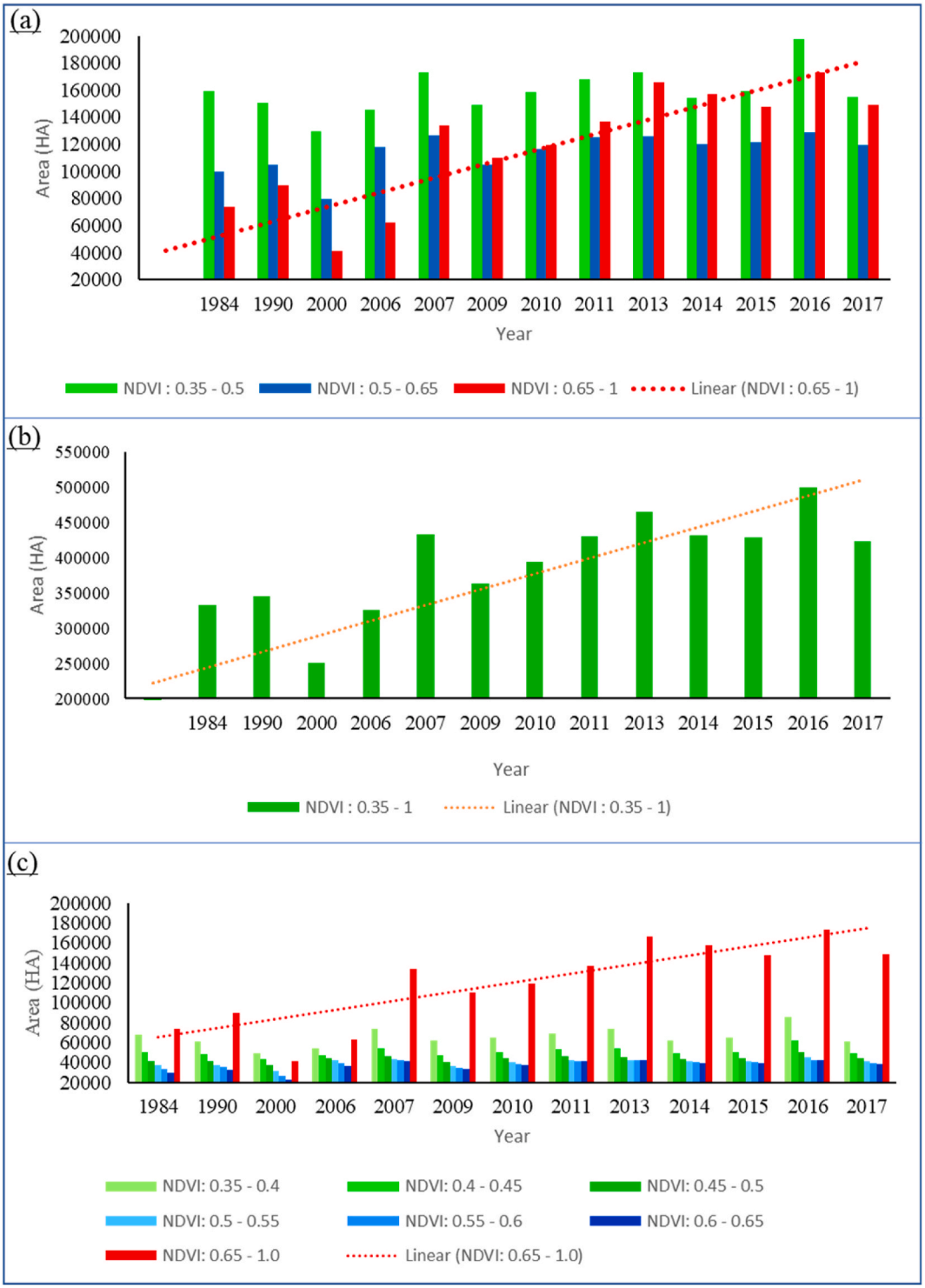

Fig. 11. Vegetation area changes in basin derived from Landsat NDVI data: (a) three-classes classification with low-vigor (NDVI 0.35–0.5), moderate (NDVI 0.5–0.65), and high-vigor vegetation (NDVI 0.65–1); (b) total vegetation area (NDVI 0.35–1); and (c) seven-classes classification with low-vigor and moderate vegetation (NDVI intervals of 0.05), and high-vigor vegetation (NDVI 0.65–1).

Fig. 13 compares vegetation density between 1984 and 2022 using two classification methods. Panel (a) employs the last non-vegetation method, while panel (b) utilizes the transition points method. The red regions in both panels highlight vegetated areas within the basin. Zoomed-in views of the Urmia Plain, Midandoab Plain, and Sarab Plain (Sections A, B, and C) show an expansion of vegetation cover over time. Additionally, Fig. 14 presents the vegetation layers derived using the fence-based thresholds. The images on the right overlay these layers on the NDVI map of the plain, illustrating the accuracy of vegetation cover delineation.

Fig. 15 summarizes changes in total vegetation area. Panel (a) shows that, according to the last non-vegetation method, the vegetation area increased from 161,463 ha in 1984 to 396,468 ha in 2022, representing a 145 % increase. Panel (b), based on the transition point (3) as the threshold, indicates a 66 % increase over the same period. Panel (c) presents results using the transition point method with the mid-point (2)

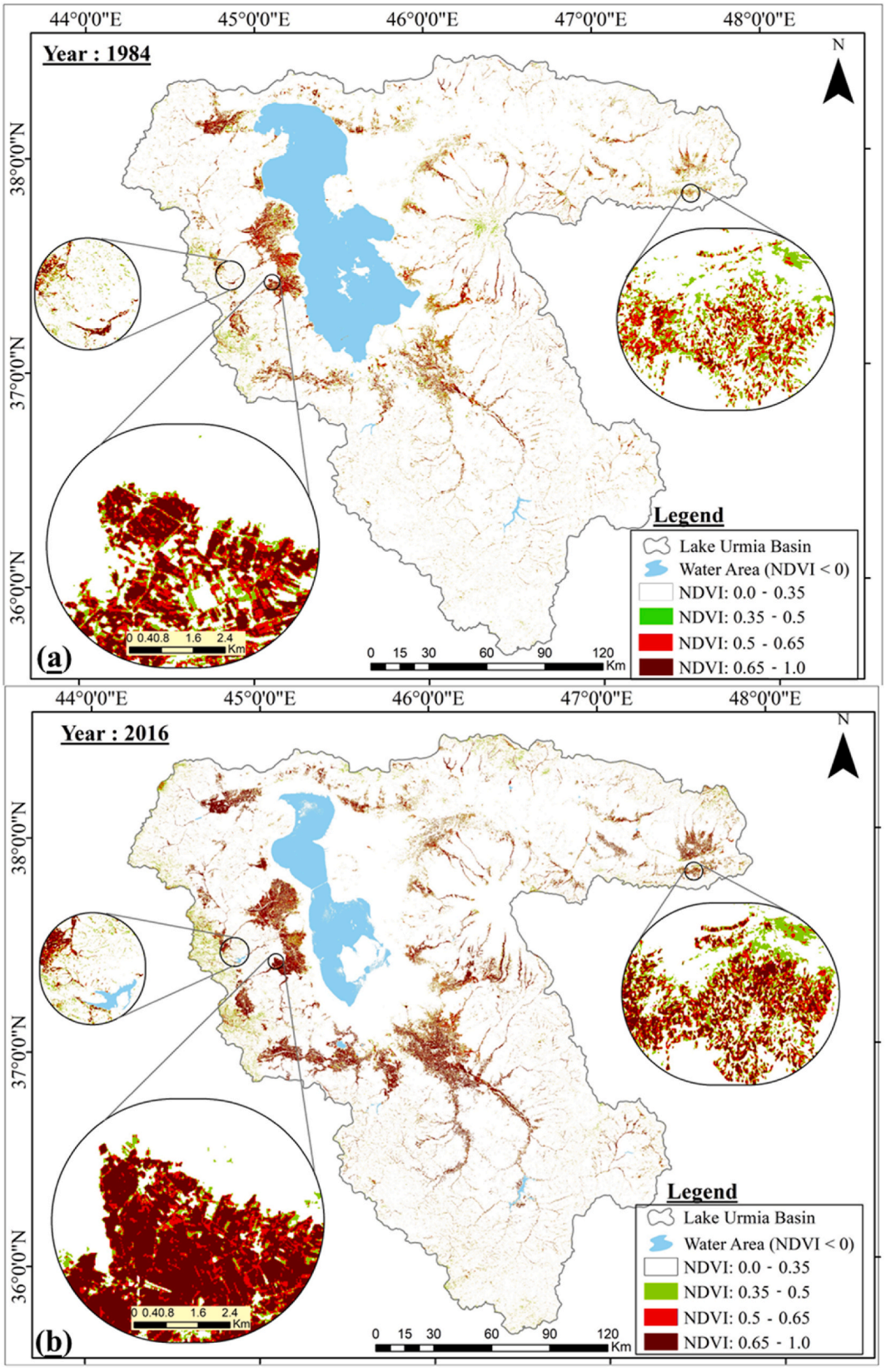

Fig. 12. Vegetation classification of the basin into three NDVI ranges (0.35–0.5, 0.5–0.65, and 0.65–1) using Landsat images for the years 1984 and 2016.

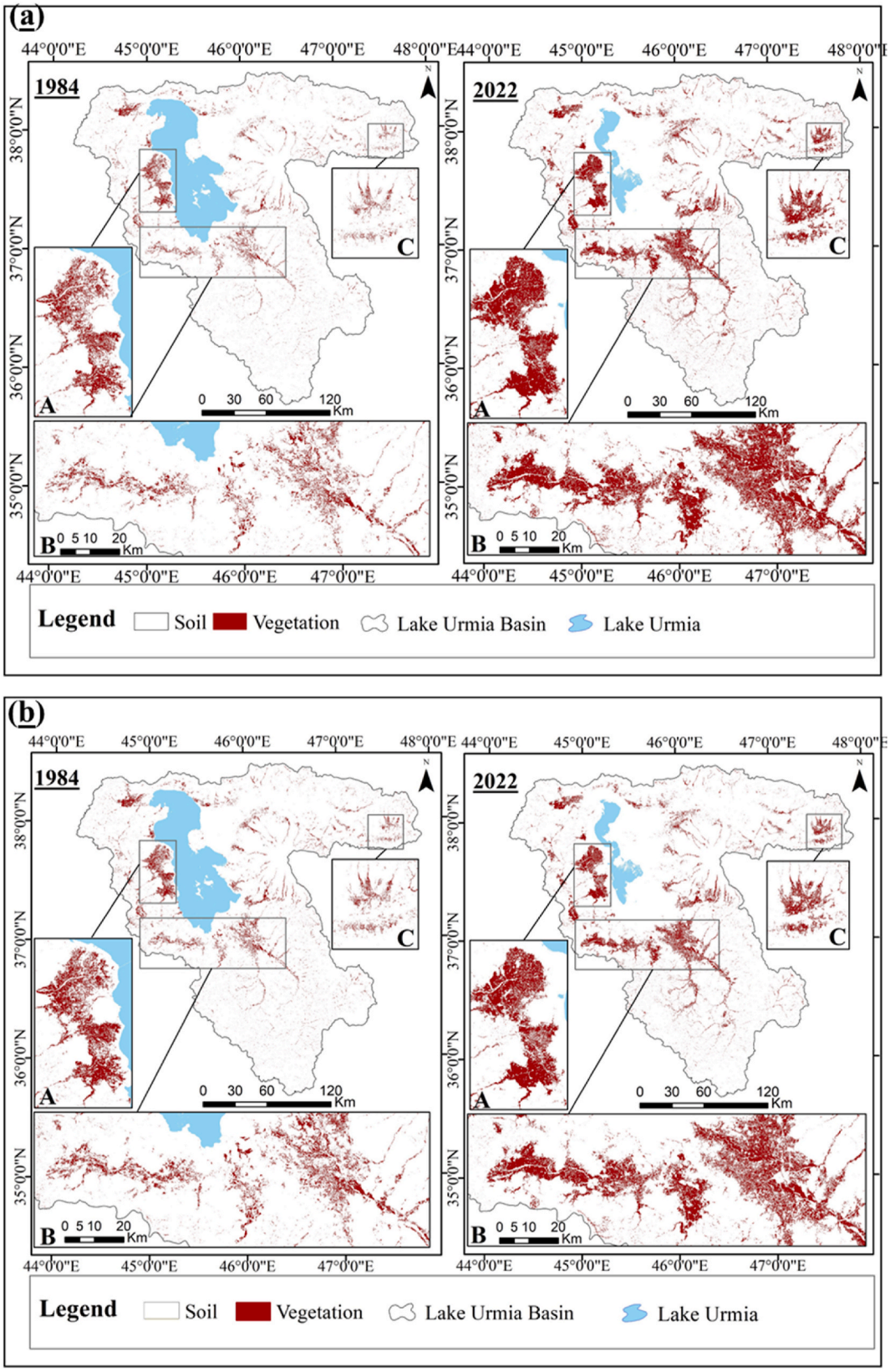

Fig. 13. Vegetation status of the basin in 1984 and 2022 derived from Landsat images using two methods: (a) the last non-vegetation pixel value method and (b) transition point method with vegetation threshold value > transition point (3).

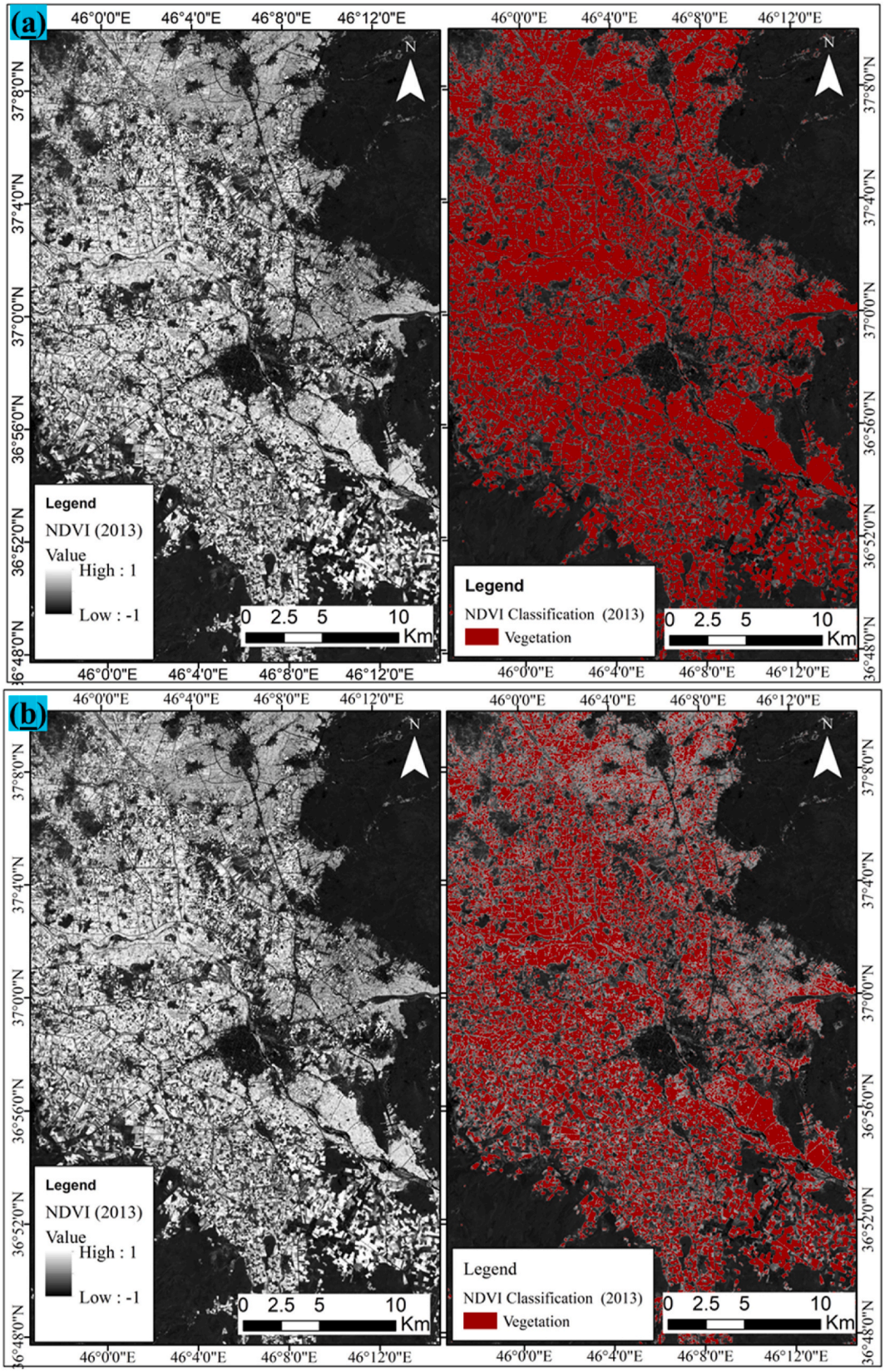

Fig. 14. Comparison of NDVI of Miandoab Plain in LUB with vegetation layers derived from fence-based thresholds: (a) Method 1 and (b) Method 2 (right panels).

Fig. 15. (a): Changes in the basin vegetation area derived from Landsat images using different classification methods: (a) last non-vegetation pixel value method; (b) transition point method with vegetation threshold at transition point (3); (c) transition point method with vegetation threshold at mid-point (2); (d) fence-based method (1); and (e) fence-based method (2).

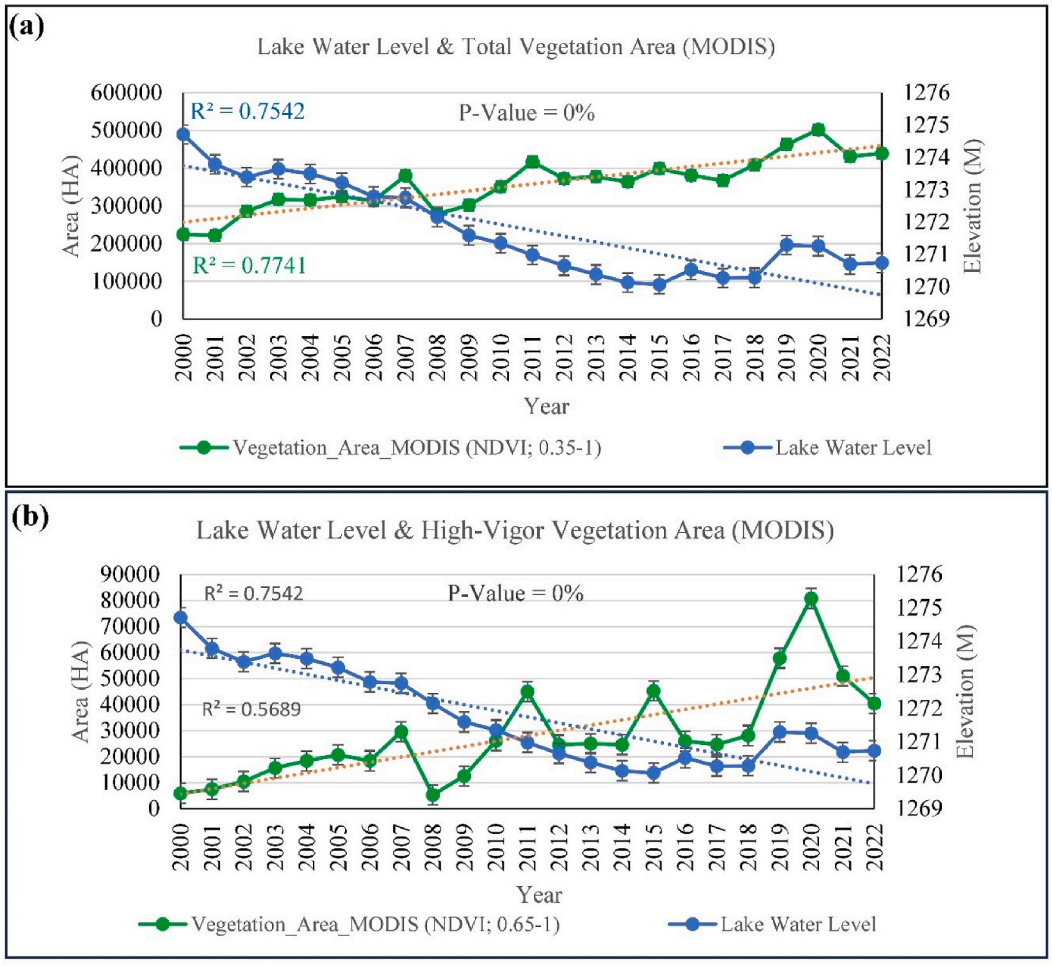

Fig. 16. Trends in simultaneous changes between lake water level and vegetation extent derived from MODIS data: (a) total vegetation (NDVI 0.35–1) and (b) high-vigor vegetation (NDVI 0.65–1).

threshold, showing a similar increasing trend but with a smaller estimated vegetation area compared to the previous method. Panels (d) and (e) compares the annual vegetation area obtained with two fence-based thresholds. Fence-based method (1) consistently shows higher vegetation area than fence-based method (2). From 1984 to 2022, the vegetation area increased by 37 % under fence-based (1) and by 42 % under fence-based (2).

The analysis of MODIS results and Lake Urmia water elevation revealed an inverse relationship between vegetation extent and lake water level over the past 24 years (Fig. 16). Landsat data further demonstrated a consistent declining trend in Lake Urmia's area over the past 38 years, with a notable acceleration observed in the last two decades. Between 1984 and 2022, the lake's water level decreased by 4.64 m, while its area shrank by 368,731 ha, equivalent to a 75 % reduction. Concurrently, vegetation cover within the basin expanded, accompanied by an expansion in water reserves behind dams. The findings also indicated a direct correlation between agricultural expansion and the reduction of the lake's area over the last 38 years (Fig. A.3).

Table 3 summarizes the percentage changes in vegetation, lake area, and reservoirs area across the study years for all methods. Moreover, Table 4 provides the quantitative values for these variables across all 15-time steps beetween1984 and 2022.

Analysis of Landsat images (1984–2022) using different classification methods showed varying vegetation growth. The method of choosing the last non-vegetative pixel indicated 146 % growth, the Transition Point method showed 67 % growth, the first fence-based method 37 %, and the second fence-based method 42 %. Thus, based on Landsat data, overall vegetation growth ranged from 37 % to 146 % (Table 3).

The results, consistent with previous studies, demonstrated a significant negative correlation between vegetation area derived from MODIS data (NDVI 0.35–1) and lake water elevation, with a correlation coefficient of −0.71 (p-value = 0.0001), indicating a strong and statistically significant relationship. Furthermore, within the NDVI range of 0.3–1, the vegetation area showed a strong negative correlation of ($r = -0.66$, p-value = 0.0005), reinforcing the robustness of these findings. Also, Table 5 displays the correlation and p-value between vegetation and lake area, with lake boundaries defined by two methods: Lake with method 2 (sampling-based water threshold) and Lake with method 1 (NDWI >0). Both approaches produced consistent patterns, confirming the reliability of the findings. Analysis of Landsat data further supported these results. The threshold-based classification, particularly the choosing of last non-vegetation pixel, the use of transition points between low-vigor and high-vigor vegetation, and the conventional NDVI method, produced correlations comparable to those of other methods, suggesting that this approach effectively captures vegetation dynamics in relation to lake elevation and area changes.

4. Discussion

4.1. *Drivers of lake shrinkage and interpretation*

To assess changes in vegetation and lake area, we also analyzed precipitation data in the LUB. Despite annual fluctuations, no significant

Table 3
Percentage growth of vegetation, lake, and reservoir areas over the study period, derived using different methods.

Year	A	B	C	D	E	F	G	H	I
1984									
1990	+18%	+14%	+18%	+19%	+4%	-	+2%	+2%	-3%
2000	-27%	+3%	+49%	+16%	-27%	-	-7%	-7%	+10%
2006	+18%	-7%	-8%	+2%	+30%	+40%	-12%	-12%	+41%
2007	+4%	-42%	-8%	-28%	+33%	+21%	0%	-2%	+39%
2009	-10%	+7%	-1%	-10%	-16%	-21%	-20%	-18%	-18%
2010	+14%	+48%	+37%	+30%	+8%	+16%	-3%	-13%	+8%
2011	+1%	+2%	-11%	+20%	+9%	+19%	-8%	-2%	+2%
2013	+6%	+12%	-3%	+8%	+8%	-9%	-24%	-35%	+1%
2014	-2%	+17%	+2%	+4%	-7%	-4%	-40%	-61%	-15%
2015	-2%	-14%	+17%	+4%	-1%	+10%	-6%	-24%	+7%
2016	+13%	-14%	-29%	-29%	+17%	-5%	+100%	+289%	+22%
2017	-12%	+12%	+31%	+11%	-15%	-4%	-18%	-40%	-17%
2020	+35%	+40%	+1%	+23%	-	+37%	+60%	+142%	+1%
2022	-8%	-9%	+25%	+2%	-	-13%	-44%	-62%	-3%
Difference 1984 & 2022	+37%	+42%	+146%	+67%	-	+96%	-60%	-75%	+70%

A = fence-based method (1) (Landsat). B = fence-based method (2) (Landsat). C = choosing last non-vegetation pixel value method (Landsat). D = transition point method (Landsat). E = conventional classification with Landsat images (NDVI 0.35–1). F = conventional classification with MODIS data (NDVI 0.35–1). J = lake area (1) (NDWI >0). H = lake area (2) (taking sample). I = Area of the reservoirs.

Table 4
Quantitative changes in vegetation, lake, and reservoir areas from 1984 to 2022. Notations are defined in Table 3.

Year\ Method	A	B	C	D	E	F	G	H	I
1984	284268	185635	161463	198315	333129	-	491597	490156	4788
1990	334844	211647	191080	236571	345012	-	503394	498562	4656
2000	243071	217060	285551	274795	250820	224361	470595	465949	5119
2006	286916	202679	263233	280036	325633	313869	415586	410414	7193
2007	298142	117764	241720	202689	433210	380053	417407	404256	9979
2009	267129	125500	239547	183005	363572	301842	335341	332406	8143
2010	305673	186052	327106	238430	394180	350784	324093	290359	8754
2011	309337	190050	291557	287151	429516	416717	299600	284988	8936
2013	328937	212920	283269	309777	464692	377515	227830	185951	9065
2014	322068	250054	289454	322696	431610	363675	136659	72862	7688
2015	316880	214012	337953	335762	427840	399018	128343	55673	8243
2016	357111	183853	238578	237977	498933	380767	256832	216636	10017
2017	313745	205963	313629	263422	423140	367217	211517	130681	8291
2020	422235	288171	318008	323524	-	501850	337578	316553	8375
2022	389670	262707	396468	330480	-	439074	189719	121425	8118

trend suggests that precipitation is a primary factor in lake reduction or cultivated area expansion (Fig. S.1). Similarly, although urban population growth has increased water demand, its relatively small share of basin-wide water use indicates it is not the main cause of declining lake levels. Regarding temperature, some studies (Alizadeh-Choobari et al., 2016; Delju et al., 2013) report recent increases of approximately 0.02–0.024 °C/year. However, data from Urmia station shows no significant deviations in August temperature from long-term averages (Barış, 2023), implying temperature alone cannot explain Lake Urmia's sharp decline.

The inverse relationship observed between MODIS vegetation results and lake water elevation, combined with the substantial decline in Lake Urmia's area and water levels (Fig. 16), suggests that human activities are significant drivers. Notably, the concurrent increase in vegetation extent and water reserves behind dams, alongside the expansion of agricultural areas, indicates that agricultural development and water consumption play critical roles in the lake's decline. These findings align with previous studies on regional hydrological changes.

The significant expansion of the high-NDVI class (0.65–1), indicative of strong, irrigated vegetation, clearly demonstrates an increase in water-intensive land use. This expansion directly correlates with heightened water consumption within the basin, offering critical evidence for how intensified agricultural practices fundamentally alter the water balance in semi-arid lake systems, pushing them towards aridity.

Table 5
Statistical relationship between results of vegetation area and lake area.

Method	Correlation		P value	
	Lake method 2	Lake method 1	Lake method 2	Lake method 1
Conventional classification with Landsat data (NDVI: 0.35–1, MODIS)	*−71 %*	*−70 %*	*0.005*	*0.006*
Choosing the last non-vegetation pixel value method	*−68 %*	*−69 %*	*0.004*	*0.004*
Transition point method (Landsat)	*−62 %*	*−63 %*	*0.01*	*0.01*
Conventional vegetation classification with MODIS data (NDVI: 0.35–1)	−46 %	−45 %	0.11	0.12
Fences-based method (1)	−38 %	−39 %	0.15	0.14
Fences-based method (2)	−32 %	−34 %	0.23	0.2

The consistent upward trend in vegetation area, robustly identified across MODIS and Landsat data by using various classification methods, not only validates our novel methodological approach but crucially highlights the pervasive and persistent nature of land-use change impacting semi-arid lake systems like Lake Urmia. This consistency, captured by both high-resolution and broad-coverage sensors, offers a reliable indicator of increasing anthropogenic water demand in such environments.

4.2. Alignment with previous findings

The inverse relationship between Lake Urmia's declining water level and area, and the increase in basin-wide vegetation cover, indicates significant shifts in regional water dynamics. These changes suggest reduced natural inflow and heightened water consumption, primarily driven by irrigation. Previous studies (Ghale et al., 2019; Parsinejad et al., 2022) report stable long-term precipitation, implying that water

Table 6
Summary of previous studies in the LUB, including their results, methodologies, limitations, and the advantages of our approach.

References	Main Sensor	Study Period	Key Changes (Veg./Lake/Reservoirs)	Main Approach	Primary Limitations
AghaKouchak et al. (2015)	Landsat	1972–2014	Lake: 88 % ↓ area, 80 % ↓ volume	Bayesian max likelihood	Lack of water demand/irrigation data; cannot quantify specific changes in reservoirs or vegetation cover quantitatively.
Ghale et al. (2019)	Landsat	1975–2014	Veg: irrigated lands +437 % ↑; lake: ~90 % ↓	MLC, NDVI	Variable veg. thresholds; accuracy affected by image quality/mixed pixels
Pooralihossein and Delavar (2020)	Landsat	1976–2007	Veg: irrigated ag. +400 % ↑; lake: ~88 % ↓	Change detection (classified maps)	Limited temporal resolution; no direct lake/reservoirs measurement; classification errors
Michel (2017)	Multisensory	1984–2014	Veg: irrigated areas +67 % ↑; lake: ~88 % ↓	Conventional classification	NDVI thresholds oversimplify variability; sensor differences/calibration issues
Alizadeh-Choobari et al. (2016)	Unspec.	1998–2011	Veg: irrigated lands tripled ↑; lake: 57.8 % ↓	Spectral indices	Changes depend on resolution/accuracy; qualitative reservoirs assessment; no specific method mentioned
Feizizadeh et al. (2022)	Landsat	1990–2020	Veg: rangelands −70.1 %↓, orchards +41.2 %↑; lake: 34.5 %↓	FOBIA	Limited temporal frequency; reservoirs not analyzed
Barış (2023)	Landsat	1967–2020	Veg: irrigated lands ~100 % ↑; lake: ~90 % ↓; reservoirs: significant ↑ after 2000	NDVI thresholds, govt. reports	NDVI may misclassify farmland as water; validation via Google Earth
Khazaei et al. (2019)	MODIS	2000–2016	Veg: NDVI +107 % ↑	NDVI thresholds	NDVI misclassification; coarse satellite resolution; temporal gaps/dataset differences
Bashirian et al. (2020)	Landsat	1984–2017	Veg: irrigated farming +14.2 % ↑; Lake: 61 % ↓; dams' capacity: significant ↑	Supervised MLC	Limited temporal frequency; cloud cover and image resolution limitations; accuracy affected by spectral similarity
Memarian Sorkhabi and Kurdpour (2024)	Landsat	1985–2021	Veg: ag. area ~110 % ↑; lake area ~32 % ↓	LSTM model	Classification limited to lake/agricultural; vegetation assumed as agriculturein mountains; dams identified visually
Fathian et al. (2016)	Landsat	1976–2011	Veg: crop land +412 % ↑; lake: 42 % ↓	Supervised MLC	Classification errors (spectral similarities/mixed pixels); reservoirs not directly measured
Naboureh et al. (2021)	Landsat	1987–2020	Veg: irrigated lands +12 % ↑; lake: 37 % ↓	Random forest (RF)	Satellite resolution limits; potential errors from spectral similarity assumption; reservoirs not measured
Esmaeilnezhad et al. (2021)	Landsat	1992–2018	Veg: rain-fed ag. +268 % ↑; irrigated croplands −12 % ↓; lake: 99 % ↓	Max. likelihood	Landsat resolution limits; misclassification due to spectral similarity, Limited temporal frequency
Chaudhari et al. (2018)	Landsat	1987–2016	Veg: ag. lands +98 % ↑; lake: 86 % ↓	Unsupervised ISODATA	reservoirs not directly measured; limited accuracy (~81.6 %); satellite resolution limits
Roushangar et al. (2023)	Landsat	2000–2020	Veg: gardens +174 % ↑; lake: 53 % ↓	Supervised SVM	Limited temporal frequency; dams not explicitly measured; misclassification risks

Notes: Our study offers several methodological advancements over prior research. We employ a hybrid approach combining conventional and innovative sample-based classification techniques to dynamically determine optimal vegetation thresholds for each year. By meticulously selecting representative pixels using NDVI layers, false-color composites, and Google Earth imagery, our method precisely accounts for inter-annual variability, leading to enhanced classification accuracy and robustness against natural variability and atmospheric influences. Furthermore, integrating 15 years of Landsat and 23 years of MODIS data (1984–2022) leverages their complementary strengths (spatial detail and frequent temporal coverage), enabling a comprehensive, long-term assessment of vegetation, lake, and reservoirs dynamics, a multifaceted approach rarely found in existing literature. Uniquely, our analysis extensively focuses on high-vigor August vegetation, which is highly dependent on spring and summer irrigation, an aspect largely unaddressed by previous studies. This research thus provides one of the most comprehensive quantitative assessments of basin-level changes, revealing, for instance, an increasing trend in vegetation cover tied to agricultural expansion.

diversion for industrial, urban, and particularly agricultural uses has been a major factor in lake decline. Agriculture, being the primary water consumer (Moghaddasi et al., 2017; Shams Ghahfarokhi and Moradian, 2023), is closely linked to the observed decrease in water levels. Additionally, dam proliferation has played a critical role. Our results show a 70 % increase in dam reservoirs since 1984, consistent with previous research (Barış, 2023; Bashirian et al., 2020; Chaudhari et al., 2018). Also, Shadkam et al. (2016) reported a 122 % increase in dam capacity from 1970 to 2010. Similarly, Michel (2017) documented a 1,300 % rise in dam numbers. This expanded water storage capacity intensifies water capture and consumption, directly contributing to the lake's diminishing volume and the transformation of its former bed into arid salt flats.

While our study establishes a long-term trend of increasing vegetation and decreasing lake area, the period between 2015 and 2020 presents a nuanced counterpoint, with a slight increase in Lake Urmia's water area and a modest decrease in vegetation. This observed short-term fluctuation, consistent with findings by Saemian et al. (2020) and attributed by Ghale et al. (2019) to factors such as higher precipitation and dam releases, serves as a crucial example of how temporary climatic shifts and policy adjustments can influence water dynamics in such semi-arid basins, even while underlying anthropogenic pressures, such as sustained agricultural expansion, continue to shape long-term trajectories. Table 6 summarizes several previous studies on vegetation, lakes, and dam reservoirs, along with our methodologies (See supplementary file for details).

4.3. Statistical analysis and interpretation of results

The significant negative correlation between vegetation area and lake water elevation ($r = -0.71$, $p < 0.0001$; $r = -0.66$, $p = 0.0005$) indicates a strong and statistically robust inverse relationship between these two variables. This finding is consistent with previous studies. When evaluating the results from Landsat data, the statistical analysis performed on various threshold values; including the last non-vegetation pixels, transition points, and conventional NDVI classification (NDVI 0.35–1), yielded acceptable performance when compared to other datasets and methods. This suggests that the classification approach employed in this study effectively captures the complex dynamics of vegetation in relation to changes in Lake Urmia's elevation and area. The statistical analyses were conducted using vegetation area estimates obtained from different methodologies, correlated against lake area data derived from two distinct approaches: Lake method 2, which utilized a lake water threshold determined by a sampling method, and Lake method 1, defined by an NDWI >0 criterion.

The observed negative correlation between lake area and vegetation cover likely stems from increased water demand for irrigation. Between 1984 and 2022, the expansion of agricultural land within the LUB, particularly for high-water-demand crops such as grapes, peaches, sugar beet, alfalfa, onions, tomatoes, and potatoes, along with the **construction of dams facilitating diversion**, significantly increased water diversion from the lake's main tributaries, consequently leading to a measurable reduction in lake area. This direct competition for water resources is a primary driver of the observed negative relationship (Ghale et al., 2019; Schulz et al., 2020).

This study aimed to find the best ways to identify vegetated (green, plant-covered, trees, agriculture) areas from satellite images by setting specific cutoff points, called thresholds, for certain spectral measurements. The goal was to accurately distinguish between areas with healthy vegetation and other land types. Since vegetation changes from year to year, due to factors like rainfall, temperature, and atmospheric conditions, these natural variations affect how plants reflect light in satellite images. Additionally, the process of capturing and processing satellite data can introduce errors or inconsistencies that might affect classification results. To address these challenges, we analyzed each satellite image separately, rather than applying a single, universal threshold across multiple years. This approach allowed us to account for the unique environmental conditions at the time each image was taken. As a result, the optimal threshold for detecting vegetation was determined individually for each image, making the classification more accurate. Overall, because vegetation quality and atmospheric conditions change over time, and because data processing can introduce errors, the study used a flexible, image-specific method. This means that the thresholds for identifying green areas varied from year to year, leading to differences in how much land was classified as vegetated in each analysis.

Our statistical analysis, confirming a strong negative correlation between vegetation expansion and lake area, solidifies the role of agricultural development and dam construction as primary drivers of Lake Urmia's desiccation. The persistent trend of these human activities, as quantified by our study, not only exacerbates water scarcity but also establishes critical pathways for environmental degradation, including saline water intrusion into aquifers and increased dust emissions, underscoring the complex socio-environmental challenges faced by arid regions.

Based on available data on irrigation practices and climate patterns in the LUB, it is estimated that 80–90 % of the lake's decline can be attributed to agricultural water use, with the remaining 10–20 % resulting from climate-related factors (Alizade Govarchin Ghale et al., 2018; Chaudhari et al., 2018; Hassanzadeh et al., 2012; Parsinejad et al., 2022).

4.4. Significance and strengths of this study

This study advances the understanding of the spatio-temporal dynamics of Lake Urmia and its basin by integrating innovative methodological approaches with comprehensive multi-sensor satellite data, thereby addressing limitations identified in prior research. Unlike earlier works such as AghaKouchak et al. (2015) and Ghale et al. (2019) which primarily relied on conventional and fixed NDVI thresholds or single-sensor analyses, our study employs several novel sampling-based classification methods that adaptively determines vegetation thresholds for each temporal observation, accounting for environmental variability and data inconsistencies. This approach enhances classification accuracy over conventional fixed-threshold methods, as evidenced by validation with Google Earth data and prior study results, and enables more precise quantification of vegetation dynamics. Furthermore, our separate analyses of Landsat and MODIS data allow us to capture both high spatial resolution details and long-term temporal trends, providing a robust long-term perspective from 1984 to 2022. In contrast to studies like Shadkam et al. (2016) and Alizadeh-Choobari et al. (2016), which separated climate and human impacts using hydrological models or trend analyses, our methodology directly correlates land cover change, water body dynamics, and anthropogenic activities through integrated remote sensing and statistical analyses, offering a more comprehensive view of basin processes. Additionally, our study uniquely combines conventional classification methods with the proposed adaptive sampling technique, thus complementing prior approaches and reducing classification uncertainties. The result is a more accurate, holistic assessment of the basin's environmental changes, providing valuable insights for targeted policy interventions.

4.5. Limitations

However, this study faces several main limitations. Its reliance on historical satellite data and a limited set of precise agricultural records for whole basin introduces uncertainties. The absence of detailed water capacity and dam reservoirs' depth measurements hampers accurate estimates of water volumes and their influence on lake levels. Variability in cloud cover and atmospheric conditions, especially in pre-2000 Landsat data, results in data inconsistencies and temporal gaps. Our study assessed overall vegetation cover within the LUB, without differentiating specific land use types such as orchards, gardens, or croplands. Incorporating these distinctions could enhance the accuracy of water usage estimates in the agricultural sector. Additionally, some biases may arise from the comparison with previous studies, which may not fully capture current land use and water management dynamics. Anthropogenic factors, such as groundwater extraction, remain insufficiently quantified, potentially underestimating their impact on lake shrinkage.

While both MODIS and Landsat data reveal vegetation expansion trends, discrepancies in the magnitude and timing of changes are possible due to differences in spatial resolution and sensor characteristics. Landsat's detailed imagery captures localized changes more accurately, whereas MODIS offers broader but more generalized insights. Although higher-resolution new satellite images, such as Sentinel, are preferable for upcoming studies in the LUB (especially in mixed land cover areas), Landsat remains valuable due to its extensive historical archive spanning several decades. Our study prioritized maximum accuracy in pixel sampling; however, future approaches should aim to reduce classification errors associated with mixed or impure pixels.

Additionally, while this study effectively demonstrates a significant inverse correlation between vegetation expansion and the shrinkage of Lake Urmia, future research should consider extending the statistical framework beyond correlation analysis. In particular, implementing multiple regression models or other multivariate approaches would allow for the inclusion of potential confounding variables, such as seasonal precipitation, temperature variations, and the spatial extent of dam reservoirs and irrigated areas. By controlling for these climatic and human-induced drivers, future studies could more robustly isolate the independent effects of vegetation expansion and irrigation practices on lake desiccation. Additionally, such analyses would enhance causal inference and strengthen policy recommendations by quantifying the relative contributions of land-use change, water management, and climate variability to hydrological decline in the basin. These advanced statistical methods could be particularly valuable when integrated with socio-economic and ground-based hydrological datasets to develop a more holistic understanding of the basin's environmental dynamics.

4.6. Suggestion for policymakers

Based on our findings, policymakers should implement vigilant land use monitoring and develop adaptive strategies to mitigate microclimate change and preserve basin ecology. Promoting water-efficient irrigation and aligning crop choices with basin water capacity, favoring less water-intensive crops, are essential. Reassessing dam policies is also critical, given their significant contribution to lake decline. Transitioning to sustainable land management and crop patterns, supported by remote sensing data, can facilitate more informed decision-making. These measures are essential for restoring water balance, supporting agricultural productivity, and enhancing resilience in water-scarce environments.

In conclusion, urgent, coordinated efforts are necessary to reverse environmental degradation in the LUB. Utilizing advanced remote sensing techniques and sustainable water management practices will be key to restoring Lake Urmia and ensuring the ecological and socio-economic stability of the region.

5. Conclusion

Our comprehensive 38-year spatio-temporal analysis (1984–2022) of the LUB, leveraging MODIS and Landsat data, offers a crucial new perspective on its critical environmental dynamics. Focusing on the interplay between surface waters (Lake Urmia and dam reservoirs) and agricultural vegetation expansion, we observed a significant decline in Lake Urmia's surface area, with a sharp decrease until 2014 followed by a partial recovery, concurrent with a long-term increase in dam reservoirs of the basin. Crucially, our analysis highlights a consistent expansion of vegetation, particularly high-vigor vegetation (representing high-value NDVI classes and thus high-water demand), directly correlating with the basin's water depletion. We conclude that this agricultural expansion is the primary driver behind Lake Urmia's diminishing water levels, a conclusion reinforced by the validation of our advanced classification methods against previous research.

The critical situation in Lake Urmia mirrors other global environmental crises, notably the Aral Sea disaster, where extensive water diversion for agriculture resulted in widespread desertification, salinization, and significant public health impacts. The similarities with other desiccating water bodies worldwide highlight the pressing need for evidence-based, sustainable water resource management to mitigate comparable ecological and societal consequences in the LUB. Ongoing agricultural expansion and escalating water consumption in the LUB are projected to induce substantial alterations in the basin's ecosystem, potentially culminating in desertification and the development of a saline environment. These projected transformations represent critical environmental and ecological challenges pertinent to arid and semi-arid regions globally, underscoring the imperative for adaptive and resilient water management strategies.

In light of these findings and our refined analytical approach, we propose the following essential policy actions:

i. Implement targeted irrigation quotas and promote water-efficient techniques for high-demand crops to curb agricultural water consumption.
ii. Establish transparent dam release protocols prioritizing environmental flows, informed by real-time data.
iii. Incentivize shifts to less water-intensive crops and support sustainable land management to counter agricultural encroachment.
iv. Enforce stricter regulations on groundwater extraction and land use planning to prevent unsustainable water use and land conversion.

These interventions, directly addressing the observed trends of increasing vegetation and the water levels of the dams alongside the decreasing lake area, are vital for the sustainable management of the basin. The long-term scope of this study provides a robust foundation for informed decision-making by officials and managers, offering a critical pathway to prevent further ecosystem deterioration and secure the region's environmental future.

CRediT authorship contribution statement

Javid Hojabri: Writing – review & editing, Writing – original draft, Visualization, Validation, Software, Methodology, Investigation, Formal analysis, Data curation, Conceptualization. **Thong Nguyen-Huy:**

Writing – review & editing, Visualization, Supervision, Conceptualization.

Declaration of generative AI in scientific writing

During the preparation of this work, the authors used ChatGPT in order to improve the readability, clarity grammar and spelling of some words and paragraphs in the manuscript. After using this tool/service, the authors reviewed and edited the content as needed and took full responsibility for the content of the published article.

Funding sources

This research did not receive any specific grant from funding agencies in the public, commercial, or not-for-profit sectors.

Declaration of competing interest

The authors declare that they have no known competing financial interests or personal relationships that could have appeared to influence the work reported in this paper.

Acknowledgements

The authors would like to acknowledge the USGS, as well as the Landsat and MODIS teams, for making the valuable data freely accessible.

Appendix A. Supplementary data

Supplementary data to this article can be found online at https://doi.org/10.1016/j.jaridenv.2025.105500.

Glossary

High vigor vegetation Displays a deep, lush greenery due to abundant chlorophyll, indicating dense, healthy growth and high photosynthetic activity, reflected in high NDVI values

Moderate vegetation Exhibits average chlorophyll content and canopy density, yielding mid-range NDVI values. It reflects balanced, ongoing growth that is neither exceptionally lush nor noticeably stressed, often representing typical seasonal or transitional-stage vegetation

Low vigor vegetation Shows muted or yellowish-greenery from reduced chlorophyll, signaling stress, sparseness, or stunted growth, resulting in lower NDVI values

Total vegetation The total area covered by vegetation within the Lake Urmia Basin, as identified by NDVI-based classification (including low-vigor vegetation, moderate vegetation, and high-vigor vegetation) over the study period

Lake area The surface area of Lake Urmia (the open water body) within the basin

Reservoirs or dam reserviors The surface water areas accumulated behind dams within the basin, interpreted as water storage in reservoir systems

Appendices.

Table A.1
Dates of the photographed days utilized for each column of Landsat images during the studied year.

	169	168	167
1984	18 Aug	27 Aug	20 Aug
1990	19 Aug	28 Aug	5 Aug
2000	14 Aug	23 Aug	1Sep*
2006	31 Aug	24 Aug	17 Aug
2007	3 Aug	11 Aug	20 Aug
2009	23 Aug	16 Aug	2 Aug
2010	10 Aug	19 Aug	12 Aug
2011	13 Aug	22 Aug	31 Aug
2013	18 Aug	11 Aug	20 Aug
2014	21 Aug	14 Aug	7 Aug
2015	8 Aug	17 Aug	10 Aug
2016	10 Aug	3 Aug	12 Aug
2017	13 Aug	22 Aug	15 Aug
2020	21 Aug	30 Aug	7 Aug
2022	11 Aug	12 Aug	13 Aug

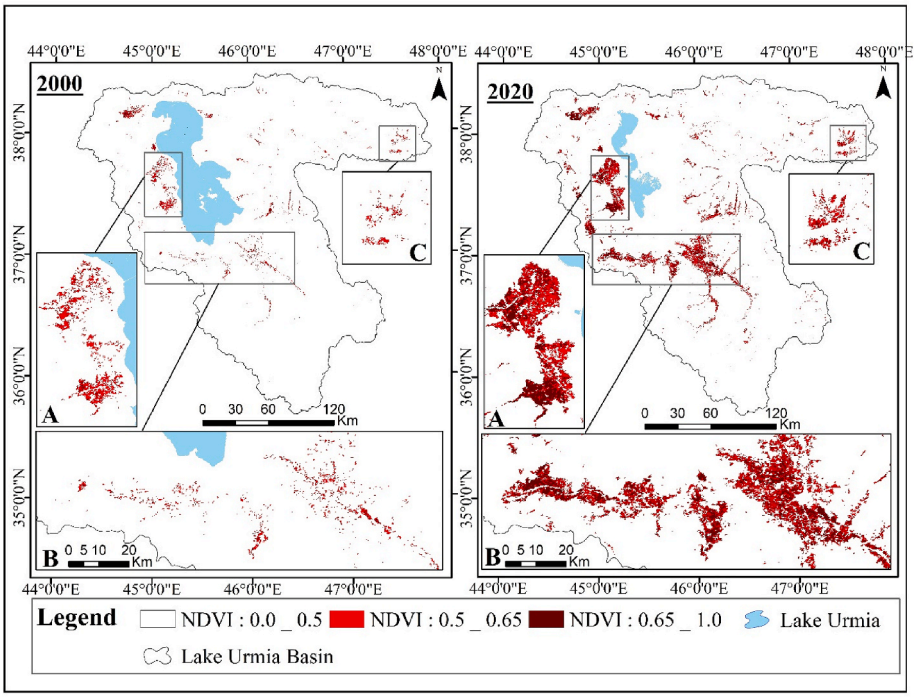

Fig. A.1. Comparison of moderate (NDVI 0.5–0.65) and high-vigor vegetation (NDVI 0.65–1) in terms of density and area between 2000 and 2020, derived from MODIS NDVI data.

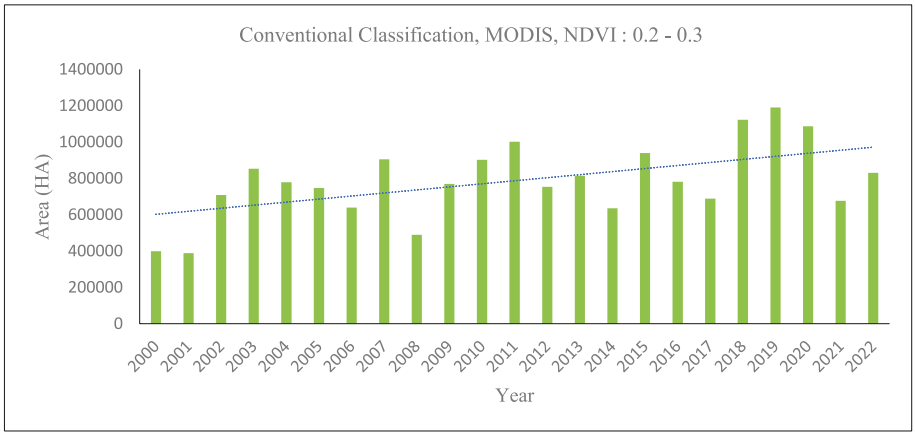

Fig. A.2. Changes in vegetation area (low-vigor vegetation) in the basin from 2000 to 2022 using MODIS products.

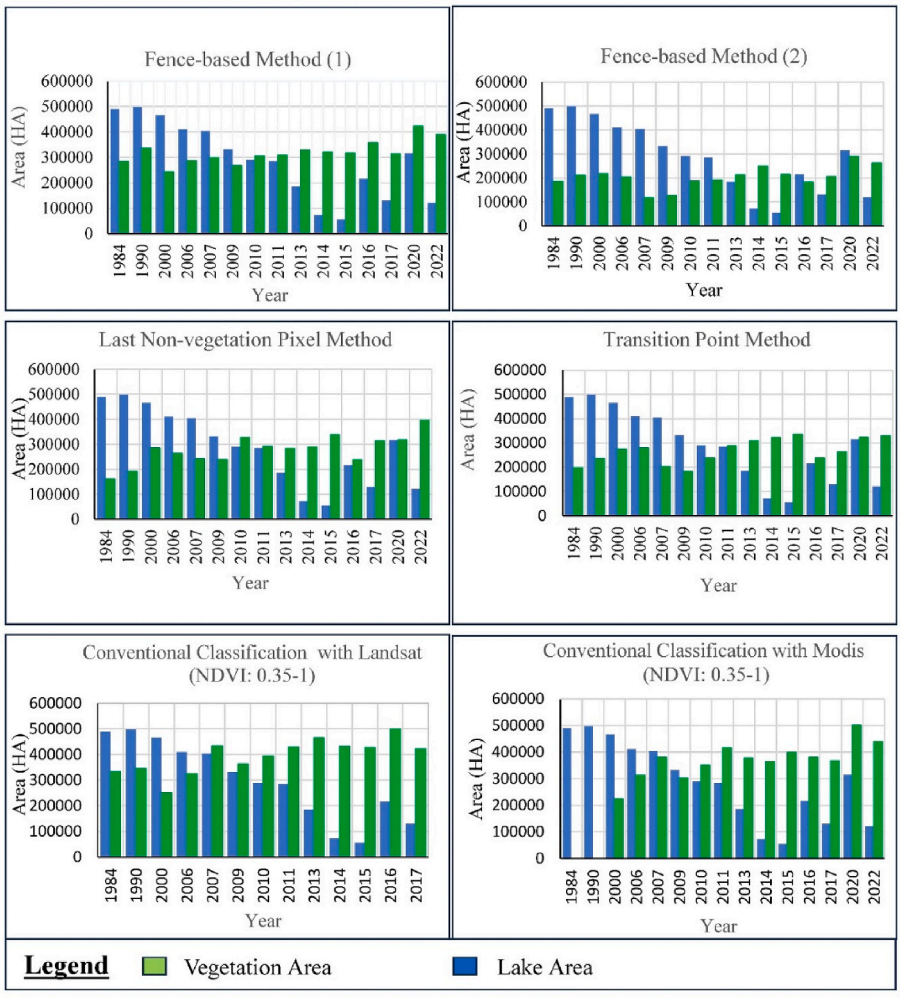

Fig. A.3. Basin lake and vegetation area changes over time, as analyzed by different methods in this study.

```
code:
For each study year:
    1. Collect NDVI pixel values for non-vegetation samples: P_non_veg
    2. Sort P_non_veg in ascending order
    3. Remove the top 10-pixel values:
        P_filtered = P_non_veg [1: length(P_non_veg) - 10]
    4. Determine threshold T:
        T = max(P_filtered)
    5. Classify all NDVI pixels in the basin:
        For each pixel NDVI_value:
            If NDVI_value >= T:
                classify as vegetation
            Else:
                classify as non-vegetation
```

Code A.1. Procedure for NDVI thresholding for last non-vegetation pixel value method.

```
Input:
 import numpy as np

def find_transition_point_3(ndvi_values, epsilon=0.005, consecutive=5):
    """
    Detect the index where slope (differences between sorted NDVI pixels)
    starts increasing sharply — this marks the transition from low-vigor vegetation
    to high-vigor vegetation (Transition Point 3).

    Parameters:
    - ndvi_values: 1D array-like, sorted NDVI pixel values (length F)
    - epsilon: float, difference threshold to detect sharp slope increase
    - consecutive: int, number of consecutive differences above epsilon

    Returns:
    - transition_index: int, pixel number where sharp increase starts (Transition Point 3)
    - transition_value: float, NDVI value at transition (Transition Point 3)
    """
    ndvi_values = np.array(ndvi_values)
    delta_y = np.diff(ndvi_values)  # differences between adjacent pixel values

    # Search for consecutive differences above epsilon
    for i in range(len(delta_y) - consecutive + 1):
        if np.all(delta_y[i:i+consecutive] > epsilon):
            transition_index = i + 1  # +1 for pixel numbering (1-based)
            transition_value = ndvi_values[transition_index]
            return transition_index, transition_value

    return None, None

# Example usage:
# sorted_ndvi = [...] # Sorted NDVI pixel values here
# idx, val = find_transition_point_3(sorted_ndvi)
# print(f"Transition Point 3 at pixel {idx} with NDVI value {val}")
```

Code A.2. Procedure for NDVI thresholding in transition point method (transition point (3) in Fig. 3).

```
Input:
import numpy as np
import matplotlib.pyplot as plt

def find_transition_point_4(ndvi_values, epsilon=0.005, window=10):
    """
    Detect the 'Transition Point 4' where low-vigor vegetation transitions to high-vigor vegetation.

    Parameters:
    - ndvi_values (list or np.array): Sorted NDVI values (from F+1 to N)
    - epsilon (float): Slope threshold for transition
    - window: Number of consecutive small differences required

    Returns:
    - transition_point_4_index: Index of transition point (relative to list)
    - transition_point_4 (float): NDVI value at transition point
    """
    ndvi_values = np.array(ndvi_values)
    dy = np.diff(ndvi_values)

    for i in range(len(dy) - window):
        if np.all(dy[i:i+window] < epsilon):
            transition_point_4_index = i + 1  # +1 shifts from dy index to pixel index
            transition_point_4_value = ndvi_values[transition_point_4_index]
            return transition_point_4_index, transition_point_4_value

    return None, None
```

Code A.3. Procedure for NDVI thresholding in transition point method (transition point (4) in Fig. 3).

```
code:
Input:
  Q1_Nv, Q3_Nv // Quartiles for non-vegetation samples
  Q1_Hvv, Q3_Hvv // Quartiles for high-vigor vegetation samples
  Q1_Lvv, Q3_Lvv // Quartiles for low-vigor vegetation samples
// Calculate fences
UpperFence_Nv = Q3_Nv + 1.5 * (Q3_Nv - Q1_Nv)
LowerFence_Hvv = Q1_Hvv - 1.5 * (Q3_Hvv - Q1_Hvv)
UpperFence_Lvv = Q3_Lvv + 1.5 * (Q3_Lvv - Q1_Lvv)

// Calculate thresholds
Threshold_Method_1 = (UpperFence_Nv + LowerFence_Hvv) / 2
Threshold_Method-2 = (UpperFence_Lvv + LowerFence_Hvv) / 2
Classify all NDVI pixels in the basin:
For each pixel NDVI_value:
//First Classification
If NDVI_value >= Threshold_Method_1:
classify as vegetation
Else:
classify as non-vegetation
//Second Classification
If NDVI_value >= Threshold_Method_2:
classify as vegetation
Else:
classify as non-vegetation
```

Code A.4. Procedure for NDVI thresholding in fence-based methods.

Data availability

Data will be made available on request.

References

AghaKouchak, A., Norouzi, H., Madani, K., Mirchi, A., Azarderakhsh, M., Nazemi, A., Nasrollahi, N., Farahmand, A., Mehran, A., Hasanzadeh, E., 2015. Aral sea syndrome desiccates Lake Urmia: call for action. J. Great Lake. Res. 41, 307–311.

Alizade Govarchin Ghale, Y., Altunkaynak, A., Unal, A., 2018. Investigation anthropogenic impacts and climate factors on drying up of Urmia Lake using water budget and drought analysis. Water Resour. Manag. 32, 325–337.

Alizadeh-Choobari, O., Ahmadi-Givi, F., Mirzaei, N., Owlad, E., 2016. Climate change and anthropogenic impacts on the rapid shrinkage of Lake Urmia. Int. J. Climatol. 36, 4276–4286.

Anchita, Zhupankhan, A., Khaibullina, Z., Kabiyev, Y., Persson, K.M., Tussupova, K., 2021. Health impact of drying aral sea: one health and socio-economical approach. Water 13, 3196.

Barani Pesyan, V., Porakrami, M., Fotouhi Mehrbani, B., 2017. The investigation of Lake Urmia drying trend and its important consequence on the surrounding settlements. Journal of Rural Research 8, 438–453.

Barhagh, S.E., Zarghami, M., Ghale, Y.A.G., Shahbazbegian, M.R., 2021. System dynamics to assess the effectiveness of restoration scenarios for the Urmia Lake: a prey-predator approach for the human-environment uncertain interactions. J. Hydrol. 593, 125891.

Barideh, R., Nasimi, F., 2022. Investigating the changes in agricultural land use and actual evapotranspiration of the Urmia Lake basin based on FAO's WaPOR database. Agric. Water Manag. 264, 107509.

Barış, M., 2023. Evaluating the impact of dam construction on extreme shrinkage of Urmia Lake using spatial data. Environ. Monit. Assess. 195, 1323.
Bashirian, F., Rahimi, D., Movahedi, S., Zakerinejad, R., 2020. Water level instability analysis of Urmia Lake Basin in the northwest of Iran. Arabian J. Geosci. 13, 1–14.
Boroughani, M., Hashemi, H., Hosseini, S.H., Pourhashemi, S., Berndtsson, R., 2019. Desiccating Lake Urmia: a new dust source of regional importance. IEEE Geoscience and Remote Sensing Letters 17, 1483–1487.
Chaudhari, S., Felfelani, F., Shin, S., Pokhrel, Y., 2018. Climate and anthropogenic contributions to the desiccation of the second largest saline lake in the twentieth century. J. Hydrol. 560, 342–353.
DAAC, 2023. L.-a.A.A.D.S.L.
Darehshouri, S., Michelsen, N., Schüth, C., Tajrishy, M., Schulz, S., 2023. Evaporation from the dried-up lake bed of Lake Urmia, Iran. Sci. Total Environ. 858, 159960.
Dehshiri, M., 2018. Biodiversity in Iran, Global Biodiversity. Apple Academic Press, pp. 165–201.
Delavar, M.A., Naderi, A., Ghorbani, Y., Mehrpouyan, A., Bakhshi, A., 2020. Soil salinity mapping by remote sensing south of Urmia Lake, Iran. Geoderma Regional 22, e00317.
Delfi, S., Mosaferi, M., Hassanvand, M.S., Maleki, S., 2019. Investigation of aerosols pollution across the eastern basin of Urmia lake using satellite remote sensing data and HYSPLIT model. J. Environ. Health Sci. Eng. 17, 1107–1120.
Delju, A., Ceylan, A., Piguet, E., Rebetez, M., 2013. Observed climate variability and change in Urmia Lake Basin, Iran. Theor. Appl. Climatol. 111, 285–296.
Djamali, M., de Beaulieu, J.-L., Shah-hosseini, M., Andrieu-Ponel, V., Ponel, P., Amini, A., Akhani, H., Leroy, S.A., Stevens, L., Lahijani, H., 2008. A late Pleistocene long pollen record from Lake Urmia, NW Iran. Quat. Res. 69, 413–420.
Eimanifar, A., Mohebbi, F., 2007. Urmia Lake (northwest Iran): a brief review. Saline Syst. 3, 5.
Elgammal, M., Ali, R., Samra, R., 2014. NDVI threshold classification for detecting vegetation cover. In: Damietta Governorate.
Emami, H., Zarei, A., 2021. Modelling lake water's surface changes using environmental and remote sensing data: a case study of lake Urmia. Remote Sens. Appl.: Society and Environment 23, 100594.
Esmaeilnezhad, R., Zeinalzadeh, K., Nazarnejad, H., Mohammadpour, M., 2021. Assessment of agricultural development preventive policies for restoration of Urmia Lake in Barandoz Basin, Iran. The Egyptian Journal of Remote Sensing and Space Science 24, 1103–1110.
Fathian, F., Dehghan, Z., Eslamian, S., 2016. Evaluating the impact of changes in land cover and climate variability on streamflow trends (case study: eastern subbasins of Lake Urmia, Iran). Int. J. Hortic. Sci. Technol. 6, 1–26.
Feizizadeh, B., Blaschke, T., Nazmfar, H., Akbari, E., Kohbanani, H.R., 2013. Monitoring land surface temperature relationship to land use/land cover from satellite imagery in Maraqeh county, Iran. J. Environ. Plann. Manag. 56, 1290–1315.
Feizizadeh, B., Lakes, T., Omarzadeh, D., Pourmoradian, S., 2023. Health effects of shrinking hyper-saline lakes: spatiotemporal modeling of the Lake Urmia drought on the local population, case study of the Shabestar county. Sci. Rep. 13, 1622.
Feizizadeh, B., Lakes, T., Omarzadeh, D., Sharifi, A., Blaschke, T., Karimzadeh, S., 2022. Scenario-based analysis of the impacts of lake drying on food production in the Lake Urmia Basin of Northern Iran. Sci. Rep. 12, 6237.
Gandhi, G.M., Parthiban, S., Thummalu, N., Christy, A., 2015. Ndvi: vegetation change detection using remote sensing and gis – a case study of vellore district. Procedia Comput. Sci. 57, 1199–1210.
Garousi, V., Najafi, A., Samadi, A., Rasouli, K., Khanaliloo, B., 2013. Environmental crisis in Lake Urmia, Iran: a systematic review of causes, negative consequences and possible solutions. In: Proceedings of the 6th International Perspective on Water Resources & the Environment (IPWE) Izmir, Turkey.
Ghaheri, M., Baghal-Vayjooee, M., Naziri, J., 1999. Lake Urmia, Iran: a summary review. Int. J. Salt Lake Res. 8, 19–22.
Ghale, Y.A.G., Baykara, M., Unal, A., 2019. Investigating the interaction between agricultural lands and Urmia Lake ecosystem using remote sensing techniques and hydro-climatic data analysis. Agric. Water Manag. 221, 566–579.
Ghale, Y.A.G., Tayanc, M., Unal, A., 2021. Dried bottom of Urmia Lake as a new source of dust in the northwestern Iran: understanding the impacts on local and regional air quality. Atmos. Environ. 262, 118635.
Hashim, H., Abd Latif, Z., Adnan, N., 2019. Urban vegetation classification with NDVI threshold value method with very high resolution (VHR) pleiades imagery. ISPRS - International Archives of the Photogrammetry, Remote Sensing and Spatial Information Sciences XLII-4/W16, 237–240.
Hassanzadeh, E., Zarghami, M., Hassanzadeh, Y., 2012. Determining the main factors in declining the Urmia Lake level by using system dynamics modeling. Water Resour. Manag. 26, 129–145.
Hemmati, M., Ahmadi, H., Hamidi, S.A., Naderkhanloo, V., 2021. Environmental effects of the causeway on water and salinity balance in Lake Urmia. Regional Studies in Marine Science 44, 101756.
Hesami, A., Amini, A., 2016. Changes in irrigated land and agricultural water use in the Lake Urmia basin. Lake Reserv. Manag. 32, 288–296.
Hojabri, J., Aydin, Y., 2025. Spatio-temporal dynamics of land surface temperature and land use and land cover changes in the Urmia Lake Basin: Exploring land-atmosphere interactions through satellite data and ground observations (2000–2023). Earth Systems and Environment 1–20. https://doi.org/10.1007/s41748-025-00808-7.
Hosseini-Moghari, S.-M., Araghinejad, S., Tourian, M.J., Ebrahimi, K., Döll, P., 2020. Quantifying the impacts of human water use and climate variations on recent drying of Lake Urmia basin: the value of different sets of spaceborne and in situ data for calibrating a global hydrological model. Hydrol. Earth Syst. Sci. 24, 1939–1956.
Jafari-Khounigh, A., Sadeghi-Bazargani, H., Haghdoost, A.A., 2022. Public perception on the health consequences of an environmental disaster: the case of Lake Urmia drying up. Med. J. Islam. Repub. Iran 36.
Jalili, S., Hamidi, S.A., Namdar Ghanbari, R., 2016. Climate variability and anthropogenic effects on Lake Urmia water level fluctuations, northwestern Iran. Hydrol. Sci. J. 61, 1759–1769.
Kanani, R., Fard, A.F., Ghorbani, M., Dinpashoh, Y., 2020. Analysis of the role of climatic and human factors in runoff variations (case study: lighvan river in Urmia Lake Basin, Iran). J. Water Clim. Change 11, 291–302.
Khazaei, B., Khatami, S., Alemohammad, S.H., Rashidi, L., Wu, C., Madani, K., Kalantari, Z., Destouni, G., Aghakouchak, A., 2019. Climatic or regionally induced by humans? Tracing hydro-climatic and land-use changes to better understand the Lake Urmia tragedy. J. Hydrol. 569, 203–217.
Koushki, R., 2013. Urmia Lake, Assessing the Portions of each Parameter on Decline of the Lake's Water Level in Different Years. Berlin.
Majediasl, M., Sangi, A., 2013. Investigation of dam construction effects without environmental assessment (case study: urmia Lake). J. Civ. Eng. Urbanism (JCEU) 3, 201–206.
Memarian Sorkhabi, O., Kurdpour, I., 2024. Assessing the impact of dams and unsustainable agricultural development on Lake Urmia drying up using multi satellite sensor and deep learning. Sustainable Water Resources Management 10, 195.
Michel, D., 2017. Iran's Impending Water Crisis, Water, Security and US Foreign Policy. Routledge, pp. 168–188.
Mirzaee, S., Nafchi, A.M., Ostovari, Y., Seifi, M., Ghorbani-Dashtaki, S., Khodaverdiloo, H., Chakherlou, S., Taghizadeh-Mehrjardi, R., Raei, B., 2024. Monitoring and assessment of spatiotemporal soil salinization in the Lake Urmia region. Environ. Monit. Assess. 196, 958.
Moghaddasi, M., Morid, S., Delavar, M., Hossaini Safa, H., 2017. Lake Urmia Basin drought risk management: a trade-off between environment and agriculture. Irrig. Drain. 66, 439–450.
Mojtahedi, A., Dadashzadeh, M., Azizkhani, M., Mohammadian, A., Almasi, R., 2022. Assessing climate and human activity effects on lake characteristics using spatio-temporal satellite data and an emotional neural network. Environ. Earth Sci. 81, 61.
Naboureh, A., Li, A., Ebrahimy, H., Bian, J., Azadbakht, M., Amani, M., Lei, G., Nan, X., 2021. Assessing the effects of irrigated agricultural expansions on Lake Urmia using multi-decadal landsat imagery and a sample migration technique within Google Earth engine. Int. J. Appl. Earth Obs. Geoinf. 105, 102607.
Parsinejad, M., Raja, O., Chehrenegar, B., 2022. Practical analysis of remote sensing estimations of water use for major crops throughout the Urmia Lake basin. Agric. Water Manag. 260, 107232.
Pengra, B., 2012. The drying of Iran's Lake Urmia and its environmental consequences. UNEP-GRID, Sioux Falls, UNEP Global Environmental Alert Service (GEAS).
Pooralihossein, S., Delavar, M., 2020. A multi-model ensemble approach for the assessment of climatic and anthropogenic impacts on river flow change. Hydrol. Sci. J. 65, 71–86.
Rahimi, A., Breuste, J., 2021. Why is Lake Urmia drying up? Prognostic modeling with land-use data and artificial neural network. Front. Environ. Sci. 9, 603916.
Roushangar, K., Aalami, M.T., Golmohammadi, H., Shahnazi, S., 2023. Monitoring and prediction of land use/land cover changes and water requirements in the basin of the Urmia Lake, Iran. Water Supply 23, 2299–2312.
Saemian, P., Elmi, O., Vishwakarma, B., Tourian, M., Sneeuw, N., 2020. Analyzing the Lake Urmia restoration progress using ground-based and spaceborne observations. Sci. Total Environ. 739, 139857.
Schröder, T., Hassanzadeh, E., Darehshouri, S., Tajrishy, M., Schulz, S., 2022. Satellite based lake bed elevation model of Lake Urmia using time series of landsat imagery. J. Great Lake. Res. 48, 1710–1717.
Schulz, S., Darehshouri, S., Hassanzadeh, E., Tajrishy, M., Schüth, C., 2020. Climate change or irrigated agriculture–what drives the water level decline of Lake Urmia. Sci. Rep. 10, 236.
Shadkam, S., Ludwig, F., van Oel, P., Kirmit, Ç., Kabat, P., 2016. Impacts of climate change and water resources development on the declining inflow into Iran's Urmia Lake. J. Great Lake. Res. 42, 942–952.
Shams Ghahfarokhi, M., Moradian, S., 2023. Investigating the causes of Lake Urmia shrinkage: climate change or anthropogenic factors? Journal of Arid Land 15, 424–438.
Shifteh Some'e, B., Ezani, A., Tabari, H., 2013. Spatiotemporal trends of aridity index in arid and semi-arid regions of Iran. Theor. Appl. Climatol. 111, 149–160.

Shirmohammadi, B., Malekian, A., Salajegheh, A., Taheri, B., Azarnivand, H., Malek, Z., Verburg, P.H., 2020. Scenario analysis for integrated water resources management under future land use change in the Urmia Lake region, Iran. Land Use Policy 90, 104299.

Sima, S., Rosenberg, D.E., Wurtsbaugh, W.A., Null, S.E., Kettenring, K.M., 2021. Managing Lake Urmia, Iran for diverse restoration objectives: moving beyond a uniform target lake level. J. Hydrol.: Reg. Stud. 35, 100812.

Taheri Dehkordi, A., Valadan Zoej, M.J., Ghasemi, H., Jafari, M., Mehran, A., 2022. Monitoring long-term spatiotemporal changes in Iran surface waters using landsat imagery. Remote Sens. 14, 4491.

Tarighi, J., Sadeghi, V., Hamedpour, H., 2023. Urmia Lake drying process modeling based on remotely sensed images and artificial neural networks. Journal of Environmental Science Studies 8, 6796–6801.

Tasumi, M., 2019. Estimating evapotranspiration using METRIC model and landsat data for better understandings of regional hydrology in the Western Urmia Lake Basin. Agric. Water Manag. 226, 105805.

Tourian, M., Elmi, O., Chen, Q., Devaraju, B., Roohi, S., Sneeuw, N., 2015. A spaceborne multisensor approach to monitor the desiccation of Lake Urmia in Iran. Rem. Sens. Environ. 156, 349–360.

Wurtsbaugh, W.A., Sima, S., 2022. Contrasting management and fates of two sister lakes: great salt Lake (USA) and Lake Urmia (Iran). Water 14, 3005.

Yazdandoost, F., Moradian, S., 2021. Climate change impacts on the streamflow of Zarrineh River, Iran. Journal of Arid Land 13, 891–904.